University of South Bohemia

Faculty of Science

# Determining the role of $F_oF_1$-ATP synthase dimers in *Trypanosoma brucei* mitochondrial biogenesis

Bachelor Thesis

**David Hollaus**

Supervisor: RNDr. Alena Panicucci Zíková, PhD

Co-Supervisor: Brian Panicucci

České Budějovice, 2020

Hollaus, D., 2020: Determining the role of $F_oF_1$-ATP synthase dimers in *Trypanosoma brucei* mitochondrial biogenesis. Bc. Thesis, in English - 70 p., Faculty of Science, University of South Bohemia, České Budějovice, Czech Republic.

**Annotation**

ATP synthase dimers have previously been identified to be major determinants of mitochondrial cristae ultrastructure. In order to determine the role of these dimers in the organellar architecture of *Trypanosoma brucei*, we performed a functional screen that identified a single *T. brucei* ATP synthase subunit that, upon depletion, destabilizes primarily dimers of the enzyme without disrupting the singular functional unit.

**Declaration**

I hereby declare that I have worked on my bachelor's thesis independently and used only the sources listed in the bibliography.

I hereby declare that, in accordance with Article 47b of Act No. 111/1998 in the valid wording, I agree with the publication of my bachelor thesis, in full form to be kept in the Faculty of Science archive, in electronic form in publicly accessible part of the IS STAG database operated by the University of South Bohemia in České Budějovice accessible through its web pages. Further, I agree to the electronic publication of the comments of my supervisor and thesis opponents and the record of the proceedings and results of the thesis defense in accordance with aforementioned Act No. 111/1998. I also agree to the comparison of the text of my thesis with the Theses.cz thesis database operated by the National Registry of University Theses and a plagiarism detection system.

České Budějovice …….. ……

David Hollaus

## Summary

The mitochondrion is often simply referred to as the powerhouse of the cell because ATP synthase generates the vast majority of the chemical energy needed to meet cellular demands. This process occurs via a coordinated chain of enzymatic activities that are housed within a special compartment of the double membrane organelle, called cristae. While it has been determined that these invaginations of the inner mitochondrial membrane are formed by the specific localization of protein complexes, like MICOS and ATP synthase, much about the biogenesis of cristae is still unknown. Here we will utilize the protist *Trypanosoma brucei*, which is an exceptional model organism because its single mitochondrion naturally undergoes drastic structural and metabolic remodeling during its life cycle. To determine the role of ATP synthase dimers in the organellar architecture, we performed a functional screen that identified a single *T. brucei* ATP synthase subunit that, upon depletion, destabilizes primarily dimers of the enzyme without disrupting the singular functional unit. This genetic cell line can now be used for various experiments that will try to resolve the importance of the ATP synthase dimer in *T. brucei* bioenergetics and cristae structure.

## Acknowledgement

I would like to thank Alena Panicucci Zíková and Brian Panicucci for providing me with the great opportunity to work at the laboratory and guiding me along the way. My special thanks goes to Brian, who has been incredibly helpful and always supported me throughout both experimentation and the writing process. Even when things got rough and there was little time to spare, he refused to make a compromise, but pulled nightshift after nightshift to provide me with the assistance I needed and more.

# Abbreviations

| | |
|---|---|
| α- | anti- |
| BF | bloodstream form |
| BN | Blue Native |
| bp | base pairs |
| cat. # | catalogue number |
| dsRNA | double stranded RNA |
| FP | forward primer |
| FW | formula weight (in g/mol) |
| IMM | inner mitochondrial membrane |
| IND# | sample from culture harvested # days after induction |
| LB | lysogeny broth |
| MCS | multiple cloning site |
| mt | mitochondrial |
| NON | sample from non-induced culture |
| nt | nucleotides |
| OMM | outer mitochondrial membrane |
| OxPhos | oxidative phosphorylation |
| pAZ | plasmid of the Alena Zíková lab |
| PCR | polymerase chain reaction |
| PF | procyclic form |
| qPCR | real-time quantitative polymerase chain reaction |
| RNAi | RNA interference |
| RP | reverse primer |
| rRNA | ribosomal RNA |

| | |
|---|---|
| RT | room temperature |
| SDS | sodium dodecyl sulfate |
| siRNA | small interfering RNA |
| SubPhos | substrate phosphorylation |
| Tb# | ATPaseTb# |
| UTR | untranslated region |
| WT | wildtype |

# Table of content

# 1 Introduction

## 1.1 Oxidative Phosphorylation and ATP

The mitochondrion is often called the powerhouse of the cell as it generates most of the ATP that is required for energy metabolism of the cell. The most efficient form of ATP production is oxidative phosphorylation (OxPhos), which is a series of enzymatic processes that generates an electrochemical proton gradient across the inner mitochondrial (mt) membrane. This proton gradient can then be converted into mechanical energy that is utilized to generate ATP. Four major membrane-bound enzyme complexes, together with the electron carriers ubiquinone and cytochrome c, comprise the respiratory chain and act together to create the proton gradient (Hatefi, 1985). The major difference between the two membrane carriers is that ubiquinone is a fat-soluble coenzyme (Lenaz & Genova, 2009), whereas cytochrome c is a hemeprotein loosely associated with the inner mt membrane (Garrido et al., 2006). The respiratory chain starts with the entrance of electrons into the membrane, by either complex I or complex II. Complex I (NADH:ubiquinone oxidoreductase) acts as a catalyzer for the oxidation of NADH and the transfer of its electrons to ubiquinone. Additionally, this enables translocation of 4 $H^+$ per oxidized NADH molecule. Complex II (succinate dehydrogenase) is a peripheral protein and a major part of the citric acid cycle. It catalyzes the oxidation of succinate to fumarate and the transfer of its electrons to ubiquinone, without additional translocation of $H^+$. Electrons are transferred from reduced ubiquinone to complex III (Ubiquinol:cytochrome c oxidoreductase), which passes them on to cytochrome c. Released energy, which stems from differences in redox potential, is utilized to pump 4 $H^+$ into the intermembrane space. Electrons are further transferred via cytochrome c to complex IV (Cytochrome c oxidase), which passes them to their final acceptor, usually oxygen, to form water. This process is again linked to the translocation of 4 $H^+$ across the membrane (Hatefi, 1985; Neupane et al., 2019). The electrochemical gradient resulting from all these translocation events creates a proton motive force across the membrane. This is the driving force of complex V (ATP synthase), which uses the motive force to generate chemical energy in the form of ATP via rotary catalysis, which completes the process known as oxidative phosphorylation (Klusch et al., 2017).

## 1.2 Structure and function of $F_oF_1$-ATP synthase

$F_oF_1$-ATP synthase generally consists of two subcomplexes, the catalytic $F_1$ head and the membrane-bound $F_o$ subcomplex. Figure 1 shows a representative image of monomeric

yeast ATP synthase, indicating the subdivisions and regions associated with the inner mt membrane (Srivastava et al., 2018). $F_1$ entirely protrudes into the mt matrix and is comprised of the catalytic head and the central stalk. In eukaryotes the catalytic head consists of 3 sets of alternating subunits α and β, forming a hexameric ring. Inserted into this ring is subunit γ of the central stalk, which extends to the inner mt membrane where it is anchored by the $F_1$ subunits δ and ε to the c-ring of the $F_o$ domain (Neupane et al., 2019). The $F_o$ domain consists of the peripheral stalk and the integral membrane proteins that constitute the c-ring, the proton pore and supernumerary subunits. The c-ring consists of 8-15 identical c-subunits that are put into rotation when a proton passes through the proton pore, which is established at the interface of subunit a and the c-ring. Such a rotation causes subunit γ to turn as well since it is anchored to the c-ring. The function of the peripheral stalk is to hold the catalytic $F_1$ head piece in place while γ and the c-ring rotate. Since the gamma subunit is asymmetrical and protrudes into the $F_1$ head, it causes conformational changes between the three pairs of α and β subunits that form the hexameric ring. It is these conformational changes that are essential for the production of ATP (Klusch et al., 2017; Neupane et al., 2019).

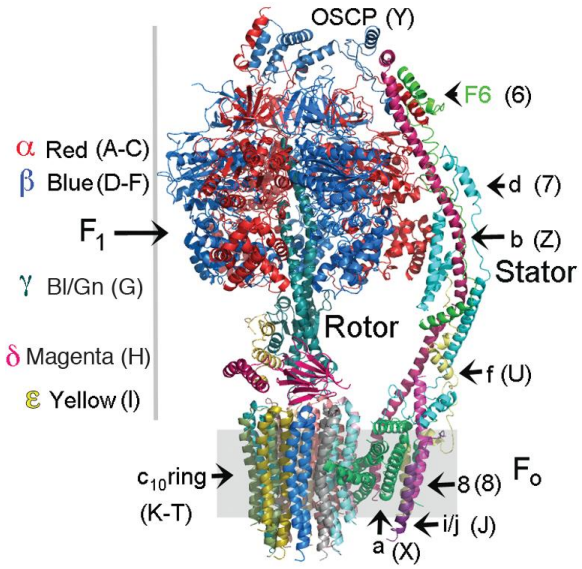


**Figure 1: Structure of monomeric yeast ATP synthase.** Shown are the catalytic $F_1$ head with the central stalk (rotor) and the $F_o$ domain with membrane-bound subunits (grey area) and the peripheral stalk (stator). Adapted from "High-resolution cryo-EM analysis of the yeast ATP synthase in a lipid membrane," by A. P. Srivastava, M. Luo, W. Zhou, J. Symersky, D. Bai, M. G. Chambers, … D. M. Mueller, 2018, *Science, 360(6389)*. Copyright 2018 by „Srivastava et al.".

One proposed mechanism for the generation of ATP in the catalytic head was made by Paul Boyer and is called the binding-change mechanism or Boyer mechanism (Figure 2). Depending on the orientation and conformation of subunit γ, each β-subunit can be present in

one of three different states: loose, open and tight. When a given subunit is in the open state, ADP and phosphate can bind to its catalytic site. Upon rotation of subunit γ in 120° steps, the β-subunit changes first into the loose state and then into the tight conformation (Baylis Scanlon, 2007). The transition from loose to tight provides enough energy to create ATP from the reaction of ADP with phosphate. Lastly, the β-subunit returns to the open conformation, where ATP is released and new substrate can bind. This is the case for all three β-subunits, thus three ATP molecules are synthesized per full turn of subunit γ (Neupane et al., 2019; Pu & Karplus, 2008; Nakamato et al., 2008). The efficiency of this process is directly linked to the number of c-subunits in the c-ring. A higher number of c-subunits means that more protons must pass through the membrane to complete a full turn of gamma (Guo et al., 2019). While the synthesis of ATP depends on the rotation of gamma in one specific direction, under the proper bioenergetic conditions, the direction of the rotation can be reversed to hydrolyze ATP. This was shown experimentally when the $H^+$ concentration in the mitochondrial matrix was greater than in the intermembrane space (Yoshida et al., 2001).

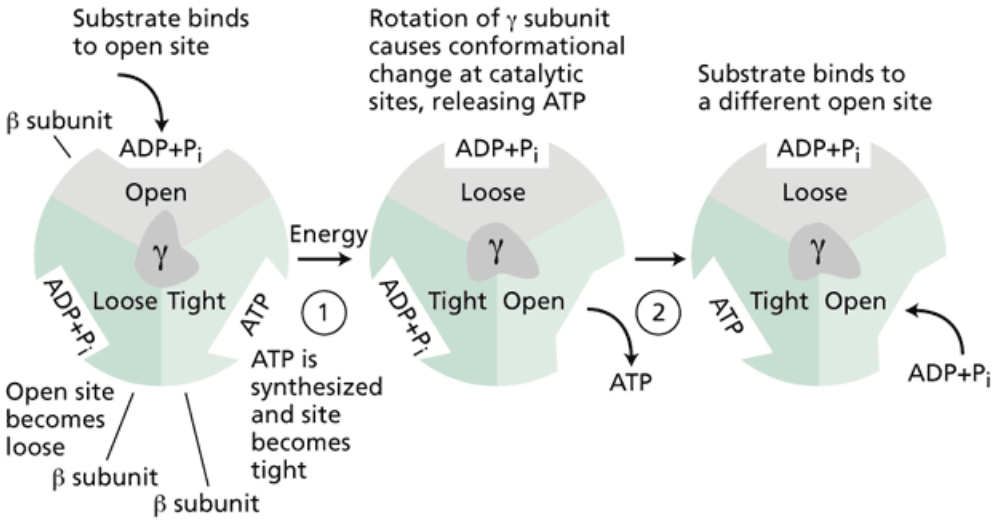


**Figure 2: Cartoon of the binding-change mechanism (Boyer mechanism).** The three β-subunits are present in different conformations, which change via rotation of subunit γ. Adapted from "ATP Synthase: Structure, Function and Inhibition." by P. Neupane, S. Bhuju, N. Thapa & H. K. Bhattarai, 2019, *Biomolecular Concepts*, *10*(1), 1–10. Copyright 2019 by „Prashant Neupane et al.".

## 1.3 ATP synthase dimerization

The $F_o$ domain also contains numerous supernumerary subunits, which are eukaryotic integral membrane proteins that are not part of the prokaryotic enzyme that was first discovered. They are involved in membrane curvature and the dimerization of ATP synthase complexes. Depending on the organism, these subunits can be highly different in their structure, resulting in dimers with different angles produced between the two joined monomers

(Kühlbrandt, 2019). It was originally believed that subunits e and g were responsible for dimerization of ATP synthase in yeast mitochondria, as deletion of these subunits resulted in a loss of dimers (Minauro-Sanmiguel et al., 2005). However, subsequent analysis of the complex via cryo-electron microscopy has shown that these are not present at the dimer interface (Guo et al., 2017). Instead, this structure (Figure 3) demonstrated that subunits a and j form the dimer interface, whereas subunits k, g, e and b create the structure that bends the lipid bilayer by ~86°. It was shown later that during assembly of the monomer, subunits e and g associate with the complex at one of the last stages, when the catalytic $F_1$ head is already bound to the peripheral stalk and is mounted to the c-ring. The only missing subunits at this stage are subunit a, which forms the proton pore via close interaction with the c-ring, and supernumerary subunits that stabilize the complex and form the dimer interface. At that point, the subunits e, g and f assemble around the membrane embedded domain of subunit b, which is part of the peripheral stalk. Only then can subunits a and j be inserted to form the complete monomer. The late insertion of subunit a is especially important because it ensures that only fully functional complexes are assembled before the proton pore is created. Lastly, it was observed that only fully assembled monomers are able to form dimers (He et al., 2018). These observations together with recent structural data suggest that subunits a and j are the ones that enable dimerization in both yeast and mammalian ATP synthase. The human structural orthologues of yeast subunits a and j are ATP6 and 6.8PL, respectively (Guo et al., 2017, He et al., 2018). Subunit k, or its human orthologue DAPIT (diabetes-associated protein in insulin-sensitive tissue), is the most peripheral of all membrane-bound subunits and probably aids in the formation of dimer rows along the cristae edges by linking adjacent ATP synthase dimers (He et al., 2018).

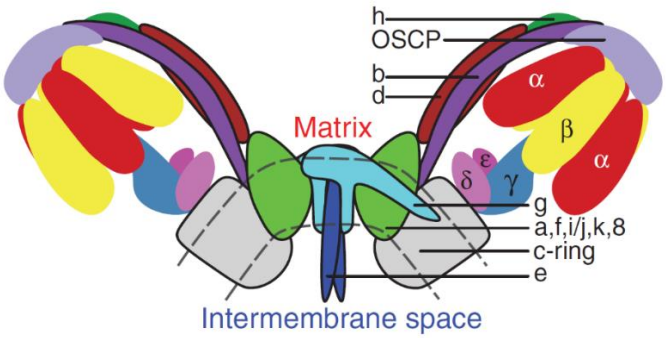


**Figure 3: Cartoon of dimeric $F_oF_1$ ATP synthase in yeast mitochondria indicating positions of subunits a, e, j and k in the region responsible for $F_o$ dimerization and membrane bending.** Adapted from „ Atomic model for the dimeric $F_o$ region of mitochondrial ATP synthase," by H. Guo, S. A. Bueler & J. L. Rubinstein, 2017, *Science*, *358*(6365), 937. Copyright 2017 by „Guo et al.".

## 1.4 Mitochondrial cristae structure

Structural and functional similarities of mitochondria and early proteobacteria suggest that the organelle originated from an endosymbiotic event in which a proteobacterium was engulfed by an amitochondrial archaeal cell. Among other features, this explains why mitochondria always have an outer and an inner membrane (Gray, 2012). The outer mt membrane (OMM) contains numerous large protein-based pores through which many small ions and molecules, including small proteins, can pass. The permeability of the inner mt membrane (IMM) is much more restricted and vastly similar to that of a prokaryotic plasma membrane. Most molecules require specific protein transporters as they traverse from the intermembrane space into the mt matrix and vice versa (O'Connor et al., 2014).

The IMM can be divided into three distinct subdomains. These are the inner boundary membrane, the cristae junctions and the cristae membrane (lumen boundary), all of which are characterized by a unique morphology and protein composition (Rabl et al., 2009). Mt cristae of different organisms can generally be classified as either lamellar (most cells of animals and fungi), tubular (unicellular green algae and ciliates) or discoid (Euglenozoa, including trypanosomes) (Kühlbrandt, 2019). Three protein complexes are thought to be major contributors to cristae structure: OPA1, the mitochondrial contact site and cristae organizing system (MICOS) and ATP synthase. OPA1 is a dynamin-related protein with increased concentrations at cristae junctions of the IMM where it protrudes into the intermembrane space. There it was proposed to form oligomers and high molecular weight complexes connecting the parts of the inner membrane forming cristae junctions. This keeps them from drifting apart and prevents the diffusion of proteins and metabolites (Quintana-Cabrera et al., 2018; Rabl et al., 2009). Similar to OPA1, the large MICOS complex is also situated at cristae junctions in the IMM. Its core component MIC60 is thought to promote IMM branching and to stabilize cristae to the inner boundary membrane by maintaining cristae junctions. Additionally, outer MICOS components establish contact sites with the OMM, which stabilizes cristae junctions and helps to sustain existing cristae (Quintana-Cabrera et al., 2018; Kaurov et al., 2017). While OPA1 and MICOS determine where the cristae invaginate, ATP synthase contributes to the membrane curvature at the cristae rims. ATP synthase is generally confined to the highly curved cristae ridges, while the supramolecular organization of respiratory chain complexes I, III and IV predominantly reside in the adjacent membrane regions (Davies et al., 2011). The ridges are caused by ATP synthase subunits involved in dimerization, which induce a strong membrane curvature at the dimer interface. ATP synthase dimers are therefore major contributors to the stability of IMM rims (Rabl et al., 2009). The

positive curvature corresponds directly to the angle between the two monomers. Since this angle varies between organisms, the complex also plays a major role in cristae structure. In organisms with lamellar cristae structure, the dimer angle is typically ~86°, whereas in tubular and discoid cristae it is lower, usually ~55° (Kühlbrandt, 2019). In addition, it has been suggested that spontaneous self-assembly of ATP synthase dimers into rows is the driving force for the folding of the IMM and thus formation of cristae in the first place (Anselmi et al., 2018). In fact, the length and curvature of ATP synthase dimer rows also varies between organisms (Kühlbrandt, 2019). Furthermore, molecular dynamics simulations suggest that no specific lipids or other proteins are required for row formation and membrane remodeling (Blum et al., 2018).

## 1.5 ATP synthase of *Trypanosoma brucei*

*Trypanosoma brucei* is a flagellated protist belonging to the group of Kinetoplastida within the phylum of Euglenozoa (Matthews, 2005; Smith et al., 2017). The name kinetoplast is derived from a characteristic structure within the mitochondrion that consists of a large mass of interlocked rings of mitochondrial DNA. The subspecies *T. brucei gambiense* and *T. brucei rhodesiense* are human pathogens, causing Human African Trypanosomiasis (HAT). The disease is transmitted by the bite of an infected tse tse fly, which is indigenous to sub-Saharan Africa. Although the number of cases per year is rather low compared to other tropical diseases, its prevalence is largely dependent on control and intervention programs, the suspension of which might lead to major outbreaks in times of political instability. New methods for the treatment of the disease are necessary since currently available drugs are old, difficult to administer and causing major side effects (Brun et al., 2010).

*T. brucei* is an extracellular parasite that undergoes significant biological changes during its life cycle (Figure 4) because it encounters very different environments as it alternates between its insect vector (procyclic form, PF) and the bloodstream of a mammalian host (bloodstream form, BF). Differentiation events include: 1) changes in gene expression and signaling pathways, 2) an exchange of surface antigens and 3) major differences in the structure and metabolism of the cell and its organelles (Fenn & Matthews, 2007). These changes are best illustrated within the single mitochondrion of the parasite, which undergoes drastic structural and metabolic remodeling. The highly branched PF mitochondrion contains abundant discoidal cristae and a functioning oxidative phosphorylation pathway. Respiratory complexes I, III and IV of the electron transport chain generate the mt membrane potential

that is coupled to ATP synthesis. In the absence of glucose, the mitochondrion relies on amino acids as major carbon sources to generate ATP via oxidative phosphorylation. If enough glucose is present, substrate phosphorylation becomes the major contributor to ATP production (Smith et al., 2017; Fenn & Matthews, 2007; Šubrtová et al., 2015). Conversely, the BF mitochondrion is significantly reduced in size and contains few to no discernable cristae. Some enzymes of the citric acid cycle are missing, as well as complex III and IV of the respiratory chain. Lacking these proton pumping respiratory complexes that maintain the mt membrane potential, the bioenergetics dictate that the ATP synthases operate in the reverse direction. Therefore, the enzyme becomes an ATPase that hydrolyzes ATP in order to generate the necessary energy to pump protons out of the mt matrix and into the intermembrane space. This requires many molecules of ATP that are generated via glycolysis, using the abundant amounts of blood glucose in the mammalian bloodstream (~ 5 mM in a healthy human). Since the mt membrane potential is required for the import of nuclear encoded proteins, ATP synthase/ATPase is thus an essential enzyme with unique properties in the infectious BF stage of the parasite (Smith et al., 2017; Šubrtová et al., 2015, Matthews, 2005).

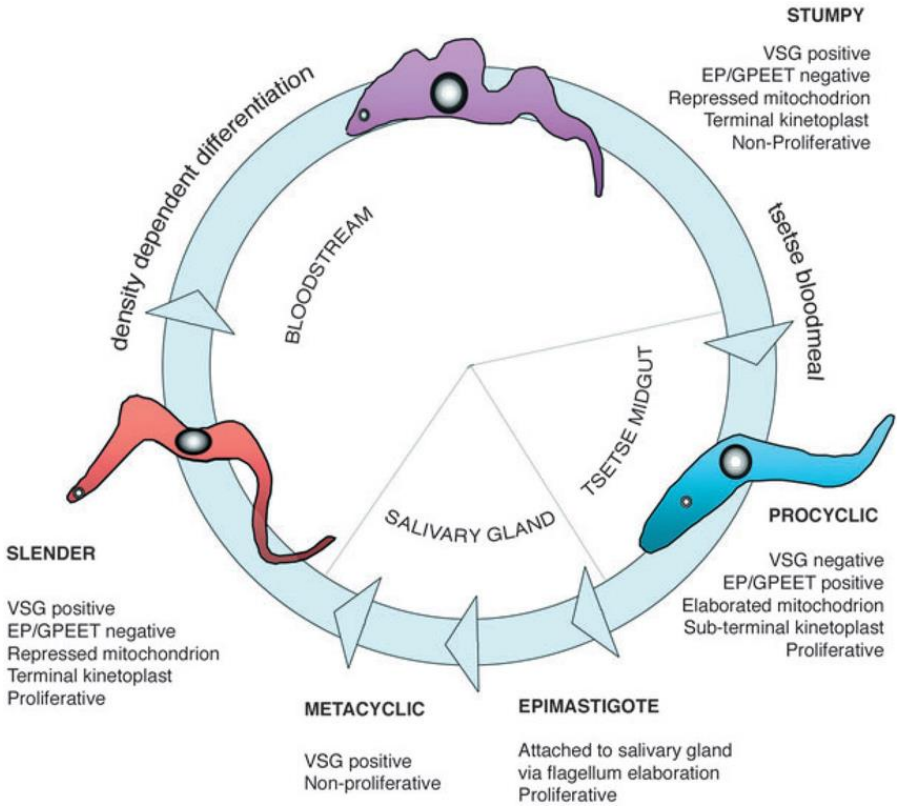


**Figure 4: Life cycle of *Trypanosoma brucei*.** In the bloodstream the parasite is present in its slender or stumpy form with repressed mitochondria and a terminal kinetoplast. Once it enters the gut of a tsetse fly the cells differentiate into their procyclic form with elaborated mitochondria and a sub-terminal kinetoplast. Adapted from „ The developmental cell biology of *Trypanosoma brucei*," by K. R. Matthews, 2005, *Journal of Cell Science, 118*(2), 13. Copyright 2005 by "The Company of Biologists Limited".

Besides the unusual task of hydrolyzing ATP at a constant rate in BF parasites, the *T. brucei* ATPase also exhibits other unique structural and functional properties. Electron cryotomography and subtomogram averaging revealed that the $F_1$ domain, which was previously thought to be highly conserved across all domains of life, forms not a six-fold ring, but rather a triangular pyramid (Mühleip et al., 2017). This special appearance is due to the presence of p18, an additional subunit with an unknown function. The *T. brucei* ATP synthase contains three copies of this novel subunit, each one attached to a typical α/β dimer (Gahura et al., 2017). Suppression of p18 expression is lethal in BF parasites, even though the catalytic sites of the complex were shown to be conventional (Montgomery et al., 2018). The subunit thus probably plays a structural role in the $F_1$ subcomplex (Gahura et al., 2017). Another peculiarity of the $F_1$ domain is that subunit α is proteolytically cleaved at two internal sites, causing the excision of an octapeptide. The resulting short N-terminal and longer C-terminal domains are both still assembled into the functional complex. The effects of this cleavage on the structure and function of the enzyme is yet unknown (Mühleip et al., 2017; Gahura et al., 2017).

The composition of the *T. brucei* ATP synthase multiprotein complex is also unique in that several of the $F_o$ domain subunits do not have obvious homologs based on the primary sequence of various known opisthokont subunits (Zíková et al., 2009). Since the original purification of the *T. brucei* complex, some of these novel Kinetoplastid subunits have also been identified in the species *Euglena gracilis*. Therefore, we can now classify all of the *T. brucei* $F_o$ domain subunits (Table 1) as either being unique to Kinetoplastids or conserved with all known Eukaryotes or Euglenozoa. The unofficial lab nomenclature is largely based on the molecular weight of the subunits. A proper analysis of the function of these subunits and their position in the complex has not yet been published, except for ATPaseTb2, which has been identified as part of the peripheral stalk (Šubrtová et al., 2015). A proposed structure of the monomeric complex is illustrated in Figure 5.

**Table 1: *T. brucei* $F_o$ domain subunits.** Different strains of *T. brucei* are used in laboratory work, here only the tritrypdb.org gene ID of the 927 strain is provided. The proposed nomenclature is based on molecular weight (MW), except for Hypo1 and Hypo2, which were just recently identified as components of the isolated complex. Known homologs of each *T. brucei* subunit are categorized as either being conserved with all known Eukaryotes, Euglenozoa or Kinetoplastids.

| AZ lab nomenclature | TriTryp 927 Gene ID | MW (kDa) | Eukaryotic conserved | Euglenozoa specific | Kinetoplastid specific |
|---|---|---|---|---|---|
| **ATPaseTb2** | Tb927.5.2930 | 43.3 | X | | |
| **OSCP** | Tb927.10.8030 | 28.8 | X | | |
| **ATPaseTb8** | Tb927.3.1690 | 17.2 | X | | |
| **ATPaseTb10** | Tb927.7.840 | 14.5 | X | | |
| **ATPaseTb11** | Tb927.4.3450 | 13.7 | X | | |
| **ATPaseTb12** | Tb927.3.2880 | 12.6 | X | | |
| **ATPaseTb15** | Tb927.11.2245 | 7.6 | X | | |
| **ATPaseTb1** | Tb927.10.520 | 46.8 | | X | |
| **ATPaseTb4** | Tb927.11.6250 | 27.6 | | X | |
| **ATPaseTb5** | Tb927.11.1270 | 20.3 | | X | |
| **ATPaseTb7** | Tb927.10.9830 | 17.2 | | X | |
| **Hypo2** | Tb927.6.590 | 12.3 | | X | |
| **ATPaseTb13** | Tb927.5.3090 | 11.7 | | X | |
| **Hypo1** | Tb927.4.720 | 19.8 | | | X |
| **ATPaseTb6** | Tb927.3.2180 | 17.9 | | | X |
| **ATPaseTb9** | Tb927.2.3610 | 16.1 | | | X |
| **ATPaseTb14** | Tb927.11.600 | 10.4 | | | X |

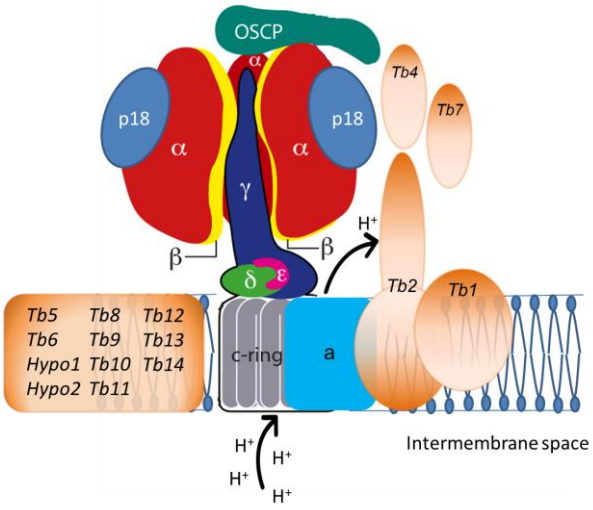


**Figure 5: Cartoon of a proposed structure of ATP synthase in *T. brucei* indicating subunits α, β and p18 as parts of the $F_1$ head, as well as OSCP, Tb1, Tb2 and ambiguous membrane-bound subunits (potentially contributing in dimer formation) as parts of the $F_o$ domain.** Adapted from "ATP Synthase: Structure, Function and Inhibition," by P. Neupane, S. Bhuju, N. Thapa, H. K. Bhattarai, 2019, *Biomolecular Concepts, 10,* 4. Copyright 2018 by "Prashant Neupane et al.".

In order to identify which of the $F_o$ subunits might be involved in the dimerization of the ATP synthase, we will need to perform a functional screen of *T. brucei* cell lines depleted of each subunit individually. While tedious, this is necessary because a recent atomic model of *E. gracilis* demonstrated that the homologs of subunits a and j do not contribute to the dimer interface. It is rather formed by Euglenozoa- and/or species-specific subunits (Mühleip et al., 2019). Ideally, the depletion of a single subunit will destabilize the ATP synthase dimers without significantly altering monomer stability and function. A regulatable cell line lacking that subunit (as by induction of RNA interference) could then be examined using transmission electron microscopy to decipher how the lack of dimers might affect cristae structure. The exploration of these fundamental properties of cristae biogenesis might help explain the drastic changes observed in the mitochondria during programmed differentiation of the parasite.

## 1.6 Aims

- Identify specific subunits responsible for dimer formation in *T. brucei*:
    - Clone specific subunits into *T. brucei* RNA interference (RNAi) vectors
    - Generate regulatable PF RNAi cell lines
    - Determine if growth is affected by RNAi induction
    - Verify RNAi efficiency by quantitative PCR analysis
    - Determine if expression levels of specific $F_oF_1$-ATP synthase subunits are affected in RNAi induced cells by steady-state Western blot analysis
    - Analyze the stability of the $F_oF_1$-ATP synthase dimers in RNAi induced cells by Blue Native gel electrophoresis
- Determine if the dimerization of ATP synthase affects the kinetics of the enzyme:
    - Measure the amount of ATP produced between non-induced and induced RNAi cells lines that specifically deplete ATP synthase dimers

# 2 Material and Methods

## 2.1 Molecular cloning

### 2.1.1 pAZ055 RNAi plasmid

To identify the function of a protein, genetics are often employed to deplete or eliminate a specific gene product. One powerful genetic tool available in *T. brucei* is RNA interference (RNAi). The aim of this procedure is to trigger the immune response of the parasite that is activated when it becomes infected with an RNA virus. Found in most eukaryotes, this RNAi pathway employs a series of enzymes to degrade the target RNA. First, the protein Dicer cleaves the double stranded RNA (dsRNA), creating small interfering RNA (siRNA) molecules. These are used by the RNA-induced silencing complex (RISC) as a template for sequence-specific cleavage of the target RNA by the protein Argonaute (Hannon, 2002). Therefore, synthesizing dsRNA molecules of 400-600 nucleotides (nt) of a particular *T. brucei* gene will lead to the degradation of that mRNA and by extension, the protein levels.

There are several different ways to generate dsRNA in *T. brucei*. We utilized the plasmid pAZ055 (Figure 6), modified in the Zíková lab from $pRPa^{iSL}$ (Alsford & Horn, 2008), which transcribes stem-loop dsRNA. This plasmid contains two multiple cloning sites (MCS) with unique restriction enzyme sites that allow a single polymerase chain reaction (PCR) amplicon of a *T. brucei* gene to be inserted into the plasmid in opposite orientations. These cloning sites are separated by a 464 nt LacZ fragment that acts as an unpaired loop between the two complementary *T. brucei* sequences that base-pair to form a double helix. Each end of the linearized plasmid contains sequence from the *T. brucei* ribosomal RNA (rRNA) spacer region, allowing the ectopic DNA to integrate into the genome by homologous recombination. A *T. brucei* rRNA promoter region engineered upstream of the stem-loop RNA ensures that the dsRNA is endogenously transcribed in the parasite. Since the depletion of the gene product may prove lethal to the genetically modified parasite, the progression of the *T. brucei* RNA polymerase I is blocked by the binding of an ectopic tetracycline repressor that binds a DNA element between the promoter and the stem-loop RNA (Poon et al., 2012). Therefore, the dsRNA transcription can be induced by the addition of tetracycline to the cell culture. This antibiotic binds the tetracycline repressor and causes a conformational change in the protein that releases it from the DNA. Finally, positive selection can be employed to ensure that selected organisms possess the plasmid DNA, which uses endogenous promoters to express the antibiotic resistance genes for ampicillin and phleomycin in *E. coli* and *T. brucei*, respectively.

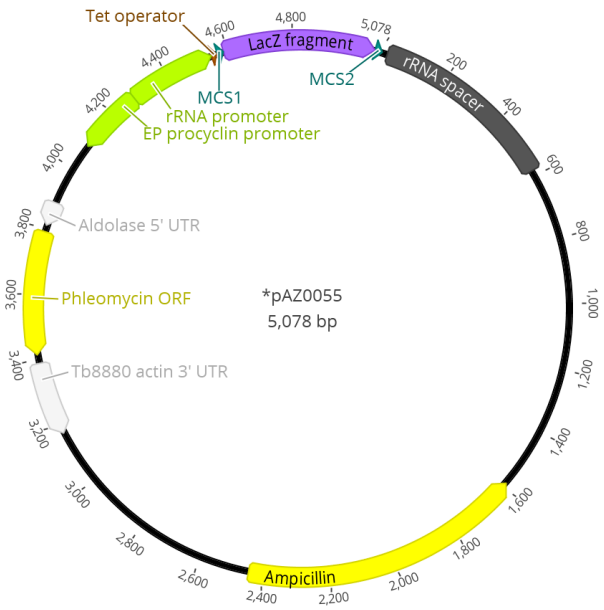


**Figure 6: Geneious schematic of the pAZ055 stem-loop RNAi vector used for depletion of target gene products in *T. brucei***. Multiple cloning sites (MCS1 and MCS 2) are denoted in blue, β-galactosidase (LacZ) coding sequence is depicted in purple, the rRNA spacer region used for homologous recombination into the *T. brucei* genome is dark grey, promoters are highlighted in green, *T. brucei* untranslated regions (UTR) are in white and the genes encoding the selectable markers are colored yellow. Software: Geneious 11.1 (https://www.geneious.com).

### 2.1.2 Primers

Oligonucleotide primers were designed to generate gene specific PCR amplicons to be cloned into the RNAi vector, as well as to verify the RNAi efficiency by quantitative PCR (qPCR). For this study, we created RNAi constructs for the following three ATPase $F_o$ subunits: ATPaseTb12 (Tb12), ATPaseTb13 (Tb13) and ATPaseTb14 (Tb14). The qPCR amplicon should be around 100 base pairs (bp) long and share no part of the sequence with the RNAi amplicon, otherwise the primers will anneal to the abundant dsRNA instead of the endogenous mRNA. The RNAi primers were designed such that the resulting amplicon is about 400 bp long, which is long enough for an effective RNAi response and still leaves some region of the gene to be analyzed by qPCR. The RNAi amplicons were comprised mostly of the gene coding sequence, but due to the small size of the targeted genes, they inevitably included a portion of the 3' untranslated regions (UTR). Since the UTRs are only predicted, care was taken to limit the size of the UTR so as to not accidently affect a downstream gene. All primers are required to contain at least a 20 bp binding region in order to avoid non-specific binding. It is also important that primers have a limited predicted secondary structure that is the result of base pairing within the primer itself. The GC-content of the forward primer (FP) and reverse primer (RP) should be approximately equal and preferably close to 50% to ensure

similar annealing temperatures within a reasonable temperature range of 50-60 °C. Nucleotides containing 2 different restriction sites were added to the 5' ends of the RNAi primers that could later be used for cloning. These restriction sites must not be encoded within the amplicon and they need to be unique for the forward and reverse primers to ensure directional cloning of the amplicon into the plasmid. Four random nucleotides were added to the 5' ends of the RNAi primers to allow better accessibility for the restriction enzymes to bind the ends of the amplicons. Once the RNAi plasmid was constructed for a targeted gene, it was sequenced to confirm the identity of the inserted amplicons. This was performed using two different primers that anneal at opposite ends of the internal LacZ DNA fragment and extend into either MCS1 or MCS2. All used primers are listen in Table 2.

**Table 2: List of primers used for cloning and qPCR.** Listed are the name, sequence, artificially added restriction sites, GC content and the total length in base pairs.

| Primer | Sequence | Restr. sites | GC (%) | length (bp) |
|---|---|---|---|---|
| Tb12 RNAi FP | TAATCTCGAGGGTACCGAATATCCGATGCATGCCGC | XhoI, KpnI | 52.8 | 36 |
| Tb12 RNAi RP | GCCGTCTAGAGGATCCACTTCGCTCTACTGCATGCA | XbaI, BamHI | 55.6 | 36 |
| Tb12 qPCR FP | AGAGTAAAAGCGCGCCTACG | | 55.0 | 20 |
| Tb12 qPCR RP | CAGTTGGAAAACCGGTAGCC | | 55.0 | 20 |
| Tb13 RNAi FP | TAATCTCGAGGGTACCGACGCCATCAAAGGAATGCC | XhoI, KpnI | 52.8 | 36 |
| Tb13 RNAi RP | GCCGTCTAGAGGATCCAGCAGCCAACAAACAGACAA | XbaI, BamHI | 52.8 | 36 |
| Tb13 qPCR FP | GCACTTCATTCTCCCGACTG | | 55.0 | 20 |
| Tb13 qPCR RP | ACATGATGTAACACCTCCGC | | 50.0 | 20 |
| Tb14 RNAi FP | TAATCTCGAGGGTACCGGGAGTACAGAAGGGCTACA | XhoI, KpnI | 52.8 | 36 |
| Tb14 RNAi RP | TAGATCTAGAGGATCCCGTGCACACCATCAGCTG | XbaI, BamHI | 52.9 | 34 |
| Tb14 qPCR FP | CAAGCCTTGCACACACTTTATG | | 45.5 | 22 |
| Tb14 qPCR RP | CCGCAAAGAAGTACGCCAC | | 57.9 | 19 |
| MCS1 seq. primer | TCCGATTTAGTGCTTTACGG | | 55.0 | 20 |
| MCS2 seq. primer | TTCAGGCTGCGCAACTGTTG | | 55.0 | 20 |

### 2.1.3 Polymerase chain reaction (PCR)

PCR is a common laboratory technique that amplifies a specific DNA fragment that can be manipulated for various molecular cloning methods. PCR exploits the ability of a thermostable DNA polymerase to synthesize new complementary DNA strands from a single

strand of the denatured DNA template. The region of amplified DNA is determined by the annealing sites of the designed primers, which get extended by the DNA polymerase in a 3' direction. To achieve this, PCR employs thermal cycling in a three-step process. First the double-stranded DNA template is denatured at temperatures between 94-98 ℃. Next, the temperature is reduced so the oligonucleotide primers can anneal to the homologous region of the DNA template. Using the template as a guide, the DNA polymerase elongates these primers at their 3' ends by incorporating the complementary deoxyribonucleotide triphosphate. Multiple repetitions of this thermal cycling exponentially amplifies the selected PCR product as each new amplicon becomes a template in the next reaction cycle.

Since gene silencing by RNAi does not require perfect sequence homology, we used Purple Taq DNA polymerase (Top-Bio, cat. # T-107). It is a thermostable non-proofreading DNA polymerase, meaning it possesses 5'→3' exonuclease activity, but no 3'→5' exonuclease proofreading activity. Additionally, it adds an adenosine overhang to the 3' end of PCR products.

In this study, a standard 50 µl PCR reaction mixture included 0.5 µl of the Tap-Purple polymerase (1 U/µl) and 5 µl of the 10x blue buffer complete supplied with the polymerase. Additionally, 200 ng genomic BF *T. brucei* DNA (2 µl of 100 ng/µl), 1 µl of a 10 mM dNTP mixture (final concentration 200 µM) and 1 µl of each selected 10 µM primer (final conc. 0.2 µM) were added to the reaction and the volume was adjusted by an appropriate amount of MilliQ water. The PCR reactions were placed into a BioRad T1000 Thermal Cycler and the program settings were entered into the machine. The reaction started with a one-time denaturation step (94 °C, 2 min). This was followed by 35 iterations of a thermo cycle that included a denaturation step (94 °C, 30 sec), a primer annealing step (55 °C, 30 sec) and DNA strand extension step (72 °C, 1 min). To ensure that all the synthesized PCR products were properly extended to create complete dsDNA molecules, a final longer extension step was included (72 °C, 7 min).

### 2.1.4 Gel electrophoresis and gel extraction

To determine whether the PCR produced a single specific amplicon of the expected size, the completed reactions were analyzed by electrophoresis on an agarose gel. Once loaded into the wells of a gel, a voltage was applied, which propels the negatively charged DNA to the positively charged anode. Since agarose is a polysaccharide polymer, it creates pores through which the DNA has to traverse. As smaller DNA molecules will move through smaller pores

more quickly than large molecules, this method resolves the various species of DNA based on size.

A 1% agarose gel (ideal for DNA molecules of 200-2000 bp) was prepared by mixing 0.7 g agarose in 700 ml 1x TAE buffer (Table 3) and then gently boiling the mixture in a microwave to fully dissolve the agarose. To visualize DNA in the gel, 1 µl of ethidium bromide, a fluorescent dye that intercalates between the two strands of dsDNA, was added. Since this dye is light sensitive, the agarose first had to be cooled to ~50 °C under running water. The gel was then quickly poured onto an acrylic tray with two rubber dams at each end and a comb with an appropriate thickness and number of wells was inserted. Once the gel solidified at room temperature (RT), it was placed into an electrophoresis chamber and immersed with 1x TAE buffer.

**Table 3: Recipe for 1 l of 1x TAE buffer.**

| Reagent | Stock/FW | Amount | Final conc. |
|---|---|---|---|
| Tris | 121.14 g/mol | 4.84 g | 40 mM |
| Glacial acetic acid | 60.05 g/mol | 1.142 ml | 20 mM |
| EDTA | 0.5 M | 2 ml | 1 mM |
| MilliQ | | fill up to 1000 ml | |

6 µl of a 10x DNA loading dye (Table 4) containing glycerol and sodium dodecyl sulfate (SDS) were added to the PCR reaction mixture (50 µl). The dense glycerol enables the PCR samples to fall into the wells of the horizontal gel, while the SDS denatures any proteins from the PCR reaction, mainly the DNA polymerase. In addition to the PCR samples, 10 µl of GeneRuler 1 kb Plus DNA Ladder (Thermo Scientific, cat. # SM1332) was loaded onto the gel so the size of the amplicon could be estimated by comparing its migration to the sizes of known DNA molecules in the ladder. The gel was run at 100 V for at least 45 min. The DNA was then visualized by taking a picture under UV exposure using the ChemiDoc™ XRS+ and the Image Lab Software (Bio-Rad).

**Table 4: Recipe for 10 ml of 10x DNA loading dye.**

| Reagent | Stock/FW | Amount | Final conc. |
|---|---|---|---|
| Glycerol | 80% | 4.9 ml | 39% |
| SDS | 10% | 500 µl | 0.5% |
| EDTA | 0.5 M | 200 µl | 10 mM |
| Xylene cyanol | 2% | 250 µl | 0.1% |
| MilliQ | | fill up to 10 ml | |

The DNA band corresponding to the expected size was extracted from the gel using the GenElute™ Gel Extraction Kit (Sigma-Aldrich, cat. # NA1111) according to the manufacturer's instructions. The excised gel slice containing the DNA fragment was solubilized in the supplied Gel Solubilization Solution and isopropanol before loading onto a binding column housed in a spin column. After centrifugation, the DNA was bound to the silica membrane. Supplied Wash Solution was passed through the membrane to remove impurities. Lastly, the DNA was eluted from the membrane by adding 50 µl Elution Solution from the kit that was preheated to 65 °C. The DNA concentration and purity was measured by a NanoDrop™ spectrophotometer (Thermo Scientific), which determines the concentration of small sample volumes (1-2 µl) by measuring UV absorption. Purity is given as a ratio of absorption values at 260 and 280 nm. The $A_{260}/A_{280}$ ratio lies around 1.8 for pure DNA samples. Abnormal ratios usually indicate some contamination, either from protein, RNA or a reagent used in the isolation process.

### 2.1.5 Restriction digest of pAZ055 and PCR amplicon

To insert the PCR amplicon into the first cloning site (MCS1), a restriction digest was performed for both the pAZ055 plasmid and the PCR product. The pAZ055 plasmid was previously isolated by another lab member from a 50 ml bacterial culture according to the manual supplied with the GenElute HP Plasmid Midiprep Kit (Sigma-Aldrich, cat. # NA0200). For the restriction digest we utilized the restriction enzymes KpnI (Thermo Scientific, cat. # ER0521) and BamHI (Thermo Scientific, cat. # ER0052), which are supplied in 50% glycerol at a concentration of 10 U/µl. Both recognize a specific 6 nt sequence (KpnI: C^CATGG, BamHI: G^GATCC) and introduce a cleavage in the DNA with a 4 nt overhang. The reaction was set up such that the final glycerol concentration was below 5% since higher glycerol concentrations can inhibit the enzyme. Thus 9 µg of plasmid DNA (41 µl of a 220 ng/µl sample) were digested in a 50 µl reaction containing 5 µl of 10x FastDigest Green Buffer (Thermo Scientific, cat. # B72) and 2 µl of each enzyme (4% final glycerol conc.). Meanwhile, all 50 µl of the PCR product were digested in a 60 µl reaction volume with 6 µl of 10x FastDigest Buffer (Thermo Scientific, cat. # B64) and 2 µl of each enzyme (3.3% final glycerol conc.). Both reaction mixtures were incubated at 37 °C for 2 hours. Subsequently the linearized plasmid was isolated by gel electrophoresis and gel extraction as described in 2.1.4. The FastDigest Green Buffer used in the plasmid digest allows for the direct loading of the sample onto the gel since it already contains a loading dye. As the PCR amplicon had already been resolved on an agarose gel, the digested PCR product was simply treated with a quick

PCR clean-up procedure that removes both the restriction enzymes and the digested nucleotides.

### 2.1.6 PCR clean-up

The digested PCR product was cleaned with the GenElute™ PCR Clean-Up Kit (Sigma-Aldrich, cat. # NA1020) according to the manufacturer's suggestions. The DNA was bound to a silica membrane inside a spin column in the presence of the provided Binding Solution. After washing, it was eluted with 50 µl of the preheated Elution Solution. The DNA concentration and purity were measured by NanoDrop™.

### 2.1.7 Ligation reaction

Since the amplicon ends contained the same restriction sites as the ones present in the multiple cloning site of the plasmid, restriction digests of the amplicon produced single-stranded DNA overhangs that were homologous to the ends of the digested plasmid. Once the sticky ends of these digested DNA fragments were allowed to anneal with each other, they could be stitched together into a single molecule using a DNA ligase that creates a phosphodiester bond between the 3'-hydroxyl and the 5'-phosphoryl of two adjacent nucleotides. It was in this framework that the PCR product was inserted into the first cloning site of pAZ055 with T4 DNA ligase (Promega, cat. # M1801). For optimal efficiency, the molarity ratio of insert:vector should be approximately 3:1, with a total of 50-200 ng vector DNA. The ligation reaction has a final volume of 10 µl, which includes 1 µl of a 10x ligation buffer and 1 µl of the T4 DNA ligase. Depending on the volume of the digested DNA fragments added to the ligation reaction, the amount of MilliQ water was adjusted to make a final volume of 10 µl. The reactions were then incubated at 4 °C for at least 12 hours (overnight). Additionally, a negative control ligation reaction was prepared for each digested vector that included the same reagents but replaced the insert DNA with MilliQ water. This control would indicate if the ligation reaction contained any non-linearized plasmid that after bacterial transformation could generate ampicillin-resistant colonies that did not contain the desired PCR insert.

### 2.1.8 Transformation

Bacterial transformation is the introduction of recombinant DNA into competent cells. Competence refers to the cell's ability to take up extracellular DNA, which can be stimulated either by heat shock or electrical shock. We employed the heat shock method and used XL-1 blue *Escherichia coli* cells that were made chemically competent by treating them with $Ca^{2+}$, which increases the permeability of the cells and enhances their uptake of DNA ("Bacterial Transformation," 2014). 50 µl frozen aliquots of these fragile cells were gently thawed on ice and then incubated for 20 min with 3 µl of the ligation reaction. The cells were then heat shocked at 42 °C for 45 sec and then allowed to recover on ice for 2 min. The transformed cells were then incubated with 250 µl of nutrient rich SOC (Super optimal broth with catabolite repression) media (Table 5) for 45 min in a shaking incubator at 37 °C. These conditions promote rapid bacterial growth, mainly due to high amounts of glucose, $SO_4^{2-}$ and $Mg^{2+}$ in the media. Once the cells obtained log-phase growth, they were spread onto agar plates (Table 6) containing lysogeny broth (LB) media and 100 µg/ml ampicillin. The plates were incubated for 12-16 hours at 37 °C. Since the solid nature of the agar restricts the movement of the bacteria, each resulting colony originated from a single dividing cell that contains the plasmid carrying the antibiotic resistance gene. This creates a colony comprised of cells with a homogenous genetic background. Great care is taken to harvest the plates after 16 hours of growth because a longer incubation period risks generating satellite colonies that do not possess the desired plasmid. These satellite colonies are able to grow in close proximity to a larger primary colony that is actively excreting the enzyme that degrades the antibiotic in the agar. These numerous but tiny satellite colonies make it almost impossible to select and analyze the positive colonies.

**Table 5: Recipe for 50 ml of SOC medium.**

| Reagent | Stock/FW | Amount | Final conc. |
|---|---|---|---|
| Yeast Extract | | 0.250 g | 0.5% |
| Tryptone | | 1 g | 2% |
| NaCl | 5 M | 100 µl | 10 mM |
| KCl | 1 M | 125 µl | 2.5 mM |
| $MgSO_4•7H_2O$ | 246.48 g/mol | 0.123 g | 10 mM |
| $MgCl_2•6H_2O$ | 203.30 g/mol | 0.102 g | 10 mM |
| Glucose | 180.15 g/mol | 0.180 g | 20 mM |
| MilliQ | | fill up to 50 ml | |

**Table 6: Recipe for LB agar plates (500 ml solution).**

| Reagent | Stock/FW | Amount | Final conc. |
|---|---|---|---|
| MilliQ | | 400 ml | |
| Tryptone | | 5 g | 1% |
| Yeast Extract | | 2.5 g | 0.5% |
| NaCl | 58.44 g/mol | 0.25 g | 8.5 mM |
| NaOH | | adjust pH to 7.3 | |
| MilliQ | | fill up to 500 ml | |
| Agar | | 7.5 g | |

### 2.1.9 Plasmid miniprep

Plasmids were isolated from 2-8 colonies (depending on the number of colonies on the negative control) to ensure that at least one will contain the plasmid with the insert. For each selected colony, the end of a sterile plastic pipet tip was passed through the colony and streaked on a replica plate before being immersed in 5 ml of liquid LB medium containing 100 µg/ml ampicillin (5 µl of 100 mg/ml stock). The liquid culture was then incubated in a shaking incubator at 37 °C for 12-16 hours.

The plasmids were isolated from the bacterial cultures using spin columns from the GenElute$^{TM}$ HP Plasmid Miniprep Kit (Sigma-Aldrich, cat. # NA0160). The *E. coli* were harvested by centrifugation (12,000 x g, 1 min, RT), resuspended in a buffer containing RNase A, subjected to an alkaline SDS-lysis (3-5 min) and then neutralized. The sample was then spun (12,000 x g, 10 min, RT) to pellet all the insoluble material, including chromosomal DNA, cell debris, proteins, lipids and SDS. The supernatant containing the plasmid DNA was loaded onto a spin column containing a silica membrane that absorbs the plasmid DNA. Additional contaminants were removed by spinning the columns with provided wash solutions. The plasmid DNA was finally eluted by centrifugation with 100 µl of elution solution that was pre-heated to 65 °C. The concentration and purity of the DNA was measured on a NanoDrop$^{TM}$.

### 2.1.10 Restriction digest analyses of isolated plasmids

In order to analyze which plasmid preps actually contained the desired MCS1 insert, a restriction digest analysis was performed using the same restriction enzymes used for the cloning. A 20 µl reaction contained MilliQ water, about 1 µg plasmid DNA, 2 µl of 10x FastDigest Green Buffer containing a loading dye (Thermo Scientific, cat. # B72) and 1 µl of

each enzyme. Due to the small amount of plasmid DNA, a 15 min incubation at 37 °C was sufficient for these rapid enzymes. Each digested plasmid was loaded onto a 1% agarose gel, which also included a 1 kb ladder for size reference. The gel was subjected to 100 V for 30-45 min before the ethidium bromide stained DNA was visualized on the ChemiDoc™. Samples containing the correct recombinant plasmid produced two bands, one at the predicted size of the linearized plasmid and another at the predicted size of the excised insert. The positive plasmid clone with the highest concentration and purity was used for downstream cloning events.

### 2.1.11 Cloning the amplicon into the second MCS

The previous steps were then repeated to insert the *T. brucei* RNAi amplicon into the MCS2 of an MCS1 positive plasmid. The PCR product was inserted in the reverse orientation using the restriction enzymes XbaI (Thermo Scientific, cat. # ER0681) and XhoI (Thermo Scientific, cat. # ER0691). Both introduce a specific 4 nt overhang (XbaI: T^CTAGA, XhoI: C^TCGAG) in the digested amplicon and plasmid. These DNA fragments were ligated and transformed into bacteria as previously described. The plasmid DNA isolated from individual bacterial clones were analyzed by two different restriction digests (KpnI & BamHI; XhoI & XbaI) to verify that the plasmid contained the RNAi insert at both cloning sites. The finalized RNAi plasmid was submitted for sequencing and later used for transfection of *T. brucei*. To preserve this plasmid, a bacterial culture started from the replica plate was frozen in glycerol. These glycerol stocks were prepared by mixing 812 µl of a liquid bacterial culture in log-phase growth with 188 µl of sterile 80% glycerol (final conc. 15%) in a cryogenic storage vial. The stocks were then stored at -80 °C.

### 2.1.12 Sequencing

After the first successful insertion of the RNAi amplicon at MCS1, the plasmid was submitted for sequencing. A 10 µl sample containing 500 ng of the plasmid and 25 pmol of a primer generated to anneal to the LacZ fragment and read through the MCS1 was prepared and mailed to the sequencing company "SEQme s.r.o.". The results were supplied online after 2-4 working days as .abi chromatogram files, which were imported into Geneious, a bioinformatics program for sequence data analysis. This software was able to align the expected *in silico* plasmid sequence with the sequencing file. The cloning was considered successful if replication errors were rare and there were no major insertions or deletions that

might significantly reduce RNAi efficiency. The final plasmid containing the RNAi amplicons at both cloning sites needed to be sequenced using a special hairpin protocol from SEQme, which required the plasmid to be linearized outside of the cloning regions.

## 2.2 Transfections

### 2.2.1 *T. brucei* cell cultures

PF *T. brucei* were grown in SDM-79 media (Table 7) containing 10% fetal bovine serum (FBS). During preparation, the media was adjusted to pH 7.3 by adding 10 M NaOH and then filter-sterilized. Unless bigger volumes are needed, PF *T. brucei* cell cultures are grown in 10 ml of media in sterile 25 cm² flasks incubated at 27 °C. To maintain the cultures at mid-log growth phase, they are kept at a concentration between $1x10^6$-$3x10^7$ cells/ml. Dense cultures ($2-3x10^7$ cells/ml) are split 1:10 under sterile conditions by discarding 9 ml of the culture into 10% bleach and adding 9 ml of fresh filtered media to the remaining 1 ml of culture. The cultures were frequently observed under a light microscope to check for a healthy morphology and possible bacterial or yeast contamination. Under normal conditions the cells grow dense again after 48 hours.

**Table 7: Recipe for 5 l of SDM-79 media.**

| Reagent | Stock/FW | Amount | Final conc. |
|---|---|---|---|
| SDM-79 powder (Life Technologies, cat. # 07490916 N) | | 127.4 g | |
| Penicillin-Streptomycin Solution (BioTech, cat. # LM-A4118100) | 100x | 50 ml | 1x |
| Hermin | 2.5 g/l | 15 ml | 833 mg/l |
| FBS | 100% | 500 ml | 10% |
| MilliQ | | fill up to 5 l | |

In order to measure cell densities, 100 µl of *T. brucei* culture were mixed well with 100 µl of Tryp Fix (Table 8) in a 1.5 ml eppendorf tube. 50 µl of these intact but unviable parasites were mixed thoroughly with 5 ml of Hemasol (HEMAX, spol. s.r.o.) in a beaker. The cells were then counted automatically by a Z2 Coulter Counter Analyzer (Beckman Coulter).

**Table 8: Recipe for 100 ml of Tryp Fix.**

| Reagent | Stock/FW | Amount | Final conc. |
|---|---|---|---|
| MilliQ | | 85 ml | |
| Saline Sodium Citrate (SSC) buffer | 20x | 5 ml | 1x |
| Formaldehyde | 37% | 10 ml | 3.7% |

For safety reasons, we used PF *T. brucei brucei*, a subspecies that infects cattle, but is incapable of causing infection in humans. To perform the RNAi studies, we employed a genetically modified Lister 427 strain that was previously transfected with genes that constitutively express the T7 RNA polymerase and a bacterial tetracycline repressor. This cell line also expresses a puromycin resistance gene that allows cell lines with these ectopic genes to be positively selected in media containing 1 µg/ml puromycin (1 µl of 1 mg/ml stock per ml media).

### 2.2.2 Plasmid preparation

A single 5 ml bacterial culture usually does not yield enough plasmid DNA for PF *T. brucei* transfections, so a pipet tip was passed through a selected colony from a replica plate and immersed into 50 ml liquid LB medium containing 100 µg/ml ampicillin (50 µl of 100 mg/ml stock). This culture was incubated at 37 °C for 12-16 hours in a shaking incubator. The plasmid was isolated using the GenElute$^{TM}$ HP Plasmid Midiprep Kit (Sigma-Aldrich, cat. # NA0200), which functions under the same principles as the Miniprep Kit, but on a larger scale. The procedures for cell harvesting, resuspension, purification using wash solutions in a spin column and elution from the column are all similar to ones described in 2.1.9. The plasmid eluted from the spin column is then however quite diluted, so it is concentrated by precipitation with 0.1 volumes of 3 M sodium acetate, pH 5.2 and 0.7 volumes of isopropanol. The insoluble DNA was pelleted by centrifugation (15,000 x g, 30 min, 4 ℃). After discarding the supernatant, the pellet was rinsed with 1.5 ml 70% ethanol and centrifuged as before for 10 min. The supernatant was again carefully decanted and the visible DNA pellet was air-dried for no longer than 10 min before it was resuspended in 100 ml elution solution pre-warmed to 65 ℃. The concentration and purity of the isolated plasmid were measured on the NanoDrop$^{TM}$.

In order to facilitate the stable integration of the plasmid DNA into the *T. brucei* genome, it was necessary to linearize the plasmid within the region of the plasmid that contained the homologous sequence to the *T. brucei* rRNA spacer region. This has the effect of generating

the recombinant DNA flanked with homologous arms that can recombine with the parasite genome. A single NotI restriction site (GC^GGCCGC) was engineered into the middle of the rRNA spacer region of the plasmid for this purpose. A 60 µl reaction digest containing MilliQ water, 20 µg of plasmid DNA, 6 µl 10x FastDigest buffer (Thermo Scientific, cat. # B64) and 5 µl of the FastDigest NotI enzyme (Thermo Scientific, cat. # ER0591) was incubated at 37 °C for 3 hours. The linearized plasmid was precipitated by the addition of 0.1 volumes 3 M sodium acetate, pH 5.2 and 2.5 volumes of 96% ethanol. After incubating at -80 °C for 30 min, the plasmid was centrifuged (15,000 x g, 30 min, 4 ℃). The supernatant was discarded and the DNA pellet was washed in 70% ethanol and then centrifuged as before, but for only 10 min. The sample was then taken into a sterile tissue culture hood where the supernatant was decanted and the plasmid allowed to air dry for no longer than 10 min. Finally, the DNA pellet was thoroughly resuspended in 30 µl sterile distilled water pre-warmed to 65 ℃. An aliquot of the sterile plasmid DNA was transferred to another 1.5 ml eppendorf tube so that it could be quantitated on the NanoDrop™ and visually inspected by gel electrophoresis. For this purpose, 1 µl of the digested plasmid was diluted in 8 µl MilliQ water and 1 µl 10x DNA loading dye. The sample was loaded onto a 0.8% agarose gel and run alongside a DNA ladder and a sample of the uncut plasmid. The resulting band should correspond to the expected size of the linearized plasmid and not indicate any traces of uncut plasmid.

### 2.2.3 Transfection of PF *T. brucei*

Transfection is the process in which recombinant DNA molecules are introduced into eukaryotic cells. For this it is necessary to open pores in the cell membrane, which is commonly done by electroporation. Since the transfection efficiency is quite low, a total of $1x10^8$ PF *T. brucei* pSMOX cells grown at mid-log phase ($6\text{-}10x10^6$ cells/ml) were harvested by centrifugation (1,300 x g, 10 min, RT). The cell pellet was washed and resuspended in sterile CytoMix buffer (Table 9) and transferred to an electroporation cuvette (0.2 cm gap) containing 12 µg sterile linearized RNAi plasmid. Electroporation was performed by an ECM 630 (BTX) electroporation system (1600 V, 25 Ω, 50 µF). This enables the uptake of extracellular linearized plasmid DNA and thereby the incorporation of the RNAi fragment and antibiotic resistance genes into the genome. Immediately after electroporation, the cells were resuspended in 6 ml SDM-79 media with 1 µg/ml puromycin (the selectable antibiotic for the parental pSMOX cell line) and incubated at 27 ℃ for 16-18 hours. At this point, another 6 ml of SDM-79 with 1 µg/ml puromycin are added to the transfected cultures, but this time the media also included the antibiotic phleomycin at a 2x working concentration, resulting in a

final 1x concentration of 2.5 µg/ml. This delay before adding the reagent to positively select for *T. brucei* harboring the recombinant RNAi DNA is necessary to allow for the integration and gene expression of the phleomycin resistance protein.

**Table 9: Recipe for CytoMix buffer.** pH adjusted to 7.6 with 5 M KOH and filter-sterilized.

| Reagent | Stock/FW | Amount | Final conc. |
|---|---|---|---|
| Hepes, pH 7.6 | 1 M | 2.5 ml | 25 mM |
| KCl | 1 M | 12 ml | 120 mM |
| $CaCl_2$ | 1 M | 15 µl | 0.15 mM |
| $KH_2PO_4/K_2HPO_4$ Buffer, pH 7.6 | 100 mM | 10 ml | 10 mM |
| EDTA | 0.5 M | 400 µl | 2 mM |
| $MgCl_2$ | 1 M | 500 µl | 5 mM |
| Glucose | 180.16 g/mol | 0.1 g | 6 mM |
| MilliQ | | fill up to 100 ml | |

### 2.2.4 Selecting positive clonal cell lines

Acquiring clonal cell lines from PF *T. brucei* is technically difficult and laborious in practice, so instead near clonal lines are derived from serial dilutions prepared in 24-well plates after the addition of the phleomycin. The first row was loaded with 2 ml of transfected cells in each well. In each of the remaining rows a 1:4 dilution was performed by adding 0.5 ml of the cell culture from the preceding row to 1.5 ml SDM-79 media containing both 1 µg/ml puromycin and 2.5 µg/ml phleomycin. The cultures were monitored and occasionally diluted for 2-3 weeks. Positive clones slowly become dense over time, with populations of cells displaying good morphology and consisting of actively dividing cells. Clonal lines that failed to integrate the recombinant DNA will have slow growth and poor morphology that manifests in skinny, twitching parasites. As positive clonal lines become dense, it is important to dilute them before they become too dense and die due to a lack of nutrients. However, it is important not to overdilute the population since it is believed that healthy cells excrete a factor that allows the culture to grow denser. Therefore, clonal lines that appeared dense enough were only split 1:2. Since dying cells can excrete lethal factors, the cells are usually split into a new well on the 24-well plate. If these diluted clonal lines continued to grow dense, they would first be split 1:3 and then 1:5. If these cells became dense again after two days of growth and they displayed good morphology, they were split 1:5 into a new 25 cm² cell culture flask. Ideally 4-5 clonal lines would be propagated from each transfection for further analysis, with a preference for the clonal lines that were derived from the most diluted cell populations on the initial plate. All other cultures were treated with 10% bleach and discarded.

## 2.3 Growth curves

One of the first phenotypes to observe when characterizing the function of a protein, is if its depletion is detrimental to the organism. Therefore, we monitored the rate of growth in the transfected cell lines that were induced for RNAi and compared that to the non-induced cells. We chose three clonal lines for each transfection because sometimes the RNAi efficiency can vary between clonal lines. Two 10 ml cultures at $5x10^6$ cells/ml of each clone were prepared in 25 cm² flasks, one of which was induced for RNAi by the addition of 10 µg tetracycline. The second culture remained non-induced and served as a reference. For the following 7 days, cell densities were recorded every 24 hours and the cultures were split back to $5x10^6$ cells/ml in a 10 ml culture. This was achieved by removing the appropriate amount of cell culture and then adding fresh SDM-79 media containing 2.5 µg/ml phleomycin and 1µg/ml puromycin so the final volume was again 10 ml. For graphical representation, first the dilution factor (Equation 1) and from that then the theoretical total cell count for each day were calculated (Equation 2). The theoretical total cell count is the number of cells the flask would contain if the flask was infinitely large and the dilutions were performed only by the addition of more media. Growth curves were then generated by plotting the total cell count against time. Of the three clonal lines analyzed for an RNAi growth effect, only one is selected for further characterization due to time and cost involved in these assays.

$$Dilution\ factor = \frac{current\ cell\ density\ (cells/ml)}{5x10^6\ cells/ml}$$

**Equation 1: Calculation of dilution factor**. e.g. a dil. factor of 4 would mean a 1:4 dilution.

$$Total\ cell\ count = cell\ density\ (cells/ml) * 10ml * all\ previous\ dilution\ factors$$

**Equation 2: Calculation of theoretical total cell count.**

## 2.4 Real-time quantitative PCR (qPCR)

### 2.4.1 Induction and harvest of *T. brucei* cultures

To determine the efficiency of each selected RNAi clonal line to deplete the target gene, it was necessary to perform quantitative PCR since we have not developed antibodies against all of the $F_o$ ATP synthase subunits. For each transfected clonal line selected, we needed to harvest cells at various time points of the RNAi induction that could then be used for total

RNA isolation. The time points were selected largely based on the growth phenotypes measured for each transfected clonal RNAi line. Ideally you choose a time point immediately before and after the growth phenotype manifests, both of which would then be compared to the non-induced culture that represents day 0. To keep the data consistent between cell lines, we chose to harvest the induced cells after 2 and 3 days of tetracycline induction. Before any RNAi induction, each clonal cell line was divided into three separate flasks and allowed to adapt to the new environment for 1-2 days. The induced day 2 and 3 flasks were then induced with 1 µg/ml tetracycline on staggered days such that the non-induced and induced day 2 and 3 cells could be harvested all on the same day. Each cell culture was monitored daily and split appropriately to ensure that a dense culture (1-3x$10^7$ cells/ml) of 20 ml was available on the day of the cell harvest. Special care was taken not to overdilute the induced day 3 culture since it typically displayed significant growth effects by this time point. A total of 2x$10^8$ cells per culture were harvested by centrifugation (1,300 x g, 10 min, 4 °C) and then resuspended in 1 ml PBS-G to maintain a physiological pH and salinity. PBS-G was made from the addition of 6 mM glucose (1.08 mg/ml) to PBS (Table 10), which is a commonly used phosphate buffer solution. This 1 ml cell suspension was then transferred to a 2.0 ml eppendorf tube.

**Table 10: Recipe for 1 l of 1xPBS**. pH adjusted to 7.4.

| Reagent | Stock/FW | Amount |
|---|---|---|
| $Na_2HPO_4$ x $12H_2O$ | 358.14 g/mol | 17.9 g |
| $NaH_2PO_4$ x $2H_2O$ | 156.0114 g/mol | 10.14 g |
| NaCl | 58.4414 g/mol | 85.0 g |
| MilliQ | | fill up to 1 l |

### 2.4.2 RNA isolation

RNA was isolated from the resuspended cells using the RNeasy® Mini Kit (Qiagen, cat. # 74104) according to the manufacturer's instructions. The cells were pelleted by centrifugation (1,300 x g, 10 min, RT) and then disrupted by the addition of 600 µl of the supplied RLT lysis buffer, which contains the general protein denaturant guanidine-thiocyanate that inactivate all RNases. The lysate was homogenized and 700 µl of 70% ethanol were added to further reduce RNA solubility. The sample was loaded onto a spin column containing a silica-based membrane that binds nucleic acids while contaminants are washed away. After three washing steps, the RNA was eluted in 50 µl RNase-free water. The RNA concentration and purity were measured on the Nanodrop™ and samples were stored at -20 °C.

### 2.4.3 DNase treatment

Since single stranded RNA is not very stable, it needs to be reverse transcribed into complementary DNA (cDNA) before it is analyzed. Therefore, we need to make sure that any trace amounts of DNA contamination in the RNA samples are degraded. We employed the TURBO DNA-free kit (Invitrogen, cat. # AM1907), which contains both DNase and an inactivation reagent in the form of DNase-binding beads that remove the enzyme after treatment. A 50 µl reaction was comprised of 10 µg of RNA, 5 µl 10x TURBO DNase buffer, 1 µl TURBO DNase enzyme (2 U) and MilliQ water. The samples were incubated at 37 °C for 60 min before another 1 µl of the DNase was added to digest the remaining DNA for an additional 30 min. Finally, 10 µl of a DNase inactivation reagent was incubated with the RNA sample for 5 min before a centrifugation step to remove the DNase enzyme. 45 µl of the RNA-enriched supernatant were carefully transferred to a fresh tube.

### 2.4.4 Reverse transcription

In order to further concentrate the RNA, samples were treated with 150 µl 96% ethanol, 5 µl 3 M sodium acetate and 1 µl glycogen and then incubated for 1 hour at -80 °C. The sodium ions were added for charge neutralization and the glycogen acts as a carrier by trapping nucleic acids when present as a precipitate ("Glycogen, RNA grade," n.d.). After spinning the RNA in a centrifuge (15,000 x g, 30 min, 4 °C), the pellets were washed with 70% ethanol and centrifuged again for 10 min. The pellets were air-dried and resuspended in 10 µl PCR-grade water preheated to 65 °C. The RNA concentration was measured on the NanoDrop™.

For cDNA synthesis, we used TaqMan® Reverse Transcription Reagents (Thermo Scientific, cat. # N8080234). A 20 µl reverse transcription reaction (+RT) consisted of MilliQ water, 2 µg RNA, 2 µl 10x RT buffer, 1.4 µl 25mM $MgCl_2$, 4 µl 10mM dNTP mix, 1 µl RNase inhibitor, 1 µl Multiscribe reverse transcriptase and 1 µl 50 µM random hexamers that served as primers. Additionally, negative samples were prepared as before, but without the reverse transcriptase (-RT), to serve as a measure for DNA contamination. cDNA was then synthesized in a thermocycler using the following program: 25 °C for 10 min, 37 °C for 30 min and 95 °C for 5 min to heat inactivate the enzyme.

### 2.4.5 qPCR

Real-time quantitative PCR is a mostly automated laboratory procedure in which the relative abundance of a PCR product is determined at the end of each cycle by measuring fluorescent light that is emitted by specialized reporters. Depending on how many cycles are required to reach a certain threshold intensity, the initial quantity of target DNA sequence is estimated. We used this technique to determine how efficiently RNAi depleted the targeted transcript by comparing the relative amount of mRNA present in the induced RNAi samples to the non-induced samples.

For each sample (both +RT and -RT at day 0, 2 and 3), designed qPCR primers were used to amplify either the specific target gene silenced by RNAi or one of two housekeeping genes (18S rRNA and β-tubulin) that serve as an internal reference between the samples. Due the sensitivity of the assay, +RT samples were analyzed in triplicates using a plate-based LightCycler 480 instrument (Roche). The SYBR Green I Master reaction mix (Roche, cat. # 4707516001) contains both the FastStart Taq DNA Polymerase and a DNA dye that fluoresces only when it binds double stranded DNA. The 20 µl qPCR reactions were assembled in a 96-well plate and consisted of 10 µl reaction mix, 4 µl each 1.5 µM qPCR primer and 2 µl of cDNA (diluted 1:10 for target genes, 1:500 for housekeeping genes). The plate was placed into the LightCycler 480 instrument and qPCR was initiated.

### 2.4.6 Processing of qPCR output

After entering sample information and the average PCR efficiency, which was determined by a linear regression program, the CFX Manager software (Bio-Rad) automatically chose a threshold fluorescence intensity and provided the crossing point (Cp-value) for all samples. This value is the cycle number at which the fluorescence intensity of the amplified target crosses the established threshold. The average Cp of each induced sample (day 2 and 3, separately) is subtracted from that of the non-induced sample for both the target gene and reference genes (ΔCp). From this, the relative abundance of the RNAi depleted transcript in the induced cells can be directly calculated (Equation 3).

$$Ratio\ treated/untreated\ = \left( \frac{Efficiency_{target}{}^{\Delta Cp\ target}}{Efficiency_{reference}{}^{\Delta Cp\ reference}} \right)$$

**Equation 3: Calculation of relative mRNA abundance.**

## 2.5 Steady state western blot analyses

### 2.5.1 Induction and harvest of *T. brucei* cultures

To determine the effect of depleting an $F_o$ ATP synthase subunit on the expression levels of other enzyme subunits, we analyzed denatured whole cell lysates by steady state western blots. These RNAi clonal lines were induced in the same way as it was described for the qPCR cultures in 2.4.1. Since we have antibodies generated against some subunits of both the $F_1$ and $F_o$ domain, we chose to analyze both early and late time points to determine the primary and secondary effects on these two different structural components of the multiprotein complex. Therefore, $5x10^7$ cells were harvested by centrifugation (1,300 x g, 10 min, 4 °C) from cultures that were either non-induced or treated with tetracycline for 2 or 4 days. The cell pellets were washed in 1 ml PBS and resuspended in 100 µl PBS and 50 µl 3x SDS-PAGE sample buffer (Table 11). The addition of the amphiphilic detergent SDS lyses both the cell membrane as well as all organellar membranes, which releases all cellular proteins. The negatively charged SDS also acts to denature all proteins by disrupting non-covalent bonds. The strong reducing agent DTT was added to disrupt disulfide bonds in proteins, while the bromophenol blue dye and dense glycerol act as a loading dye. The samples were incubated at 97 °C for 7 min to complete the denaturation process and reduce viscosity.

**Table 11: Recipe for 50 ml of 3x SDS-PAGE sample buffer.**

| Reagent | Stock/FW | Amount | Final conc. |
|---|---|---|---|
| Sodium dodecyl sulfate (SDS) | 288.37 g/mol | 3.0 g | 6% |
| Dithiothreitol (DTT) | 154.25 g/mol | 2.31 g | 0.3 M |
| Tris pH 6.8 | 1 M | 7.5 ml | 0.15 M |
| Glycerol | 80% | 18.75 ml | 30% |
| Bromophenol blue | 2% | 500 µl | 0.02% |
| MilliQ | | fill up to 50 ml | |

### 2.5.2 SDS-PAGE

Polyacrylamide gel electrophoresis (PAGE) is generally used to separate macromolecules in a mixture, such as proteins from a whole cell lysate, based on their size and charge by applying a voltage through an acrylamide gel. In the case of SDS-PAGE, proteins are previously denatured to eliminate any protein-protein interactions, especially those needed to form multiprotein complexes. The high concentration of SDS also provides proteins with a large negative charge, thereby eliminating the charge contribution. This allows for the migration of each protein through the acrylamide matrix to be based solely on their size. Since we wanted to analyze proteins of various sizes in our complex mixture, we resolved

the whole cell lysates on Mini-Protean TGX Stain-Free Precast Gels with a 4-20% gradient (Bio-Rad, cat. # 4568094). The anode and cathode space of the gel apparatus were filled with 1x SDS-PAGE running buffer (Table 12). The gel was loaded with 4 µl of a PageRuler Prestained Protein Ladder (Thermo Scientific, cat. # 26616), which was followed by 15 µl of each protein sample (whole cell lysate from $5x10^6$ cells). The gel was run at 120 V until the dye front reached the lower edge of the gel (1-2 hours).

**Table 12: Recipe for 1 l of 10x SDS-PAGE running buffer.** Diluted 1:10 for 1x concentration.

| Reagent | Stock/FW | Amount | Final conc. |
|---|---|---|---|
| Tris | 121.14 g/mol | 30.3 g | 0.25 M |
| Glycine | 75.07 g/mol | 144.4 g | 1.9 M |
| SDS | 288.37 g/mol | 10 g | 1% |
| MilliQ | | fill up to 1 l | |

### 2.5.3 Electroblotting onto a PVDF membrane

For better handling, the proteins were horizontally transferred onto a membrane, which was previously activated by soaking in methanol, MilliQ and 1x Transfer buffer (Table 13). The blotting sandwich was prepared in the following order: cathode cassette, sponge, filter paper, gel, membrane, filter paper, sponge, anode cassette. The blotting apparatus was filled with cold 1x Transfer buffer and the proteins were transferred by applying 90 V for 90 min.

**Table 13: Recipe for 1 l of 10x Transfer Buffer.**

| Reagent | Stock/FW | Amount | Final conc. |
|---|---|---|---|
| Glycine | 75.07 g/mol | 29.3 g | 0.4 M |
| Tris | 121.14 g/mol | 58.15 g | 0.48 M |
| MilliQ | | fill up to 1 l | |

### 2.5.4 Probing with antibodies

In order to reduce unspecific binding of antibodies, the membranes were incubated in 45 ml blocking solution overnight and then for an additional 30 min in rotation the next morning. Blocking solution was prepared by dissolving 3 g skim milk in 60 ml PBS-T. PBS-T was made by adding 500 µl Tween 20 to 1 l PBS. Next, the membrane was rotated for 1 hour in a 5 ml blocking solution containing one of the six polyclonal rabbit antibodies raised against one of the *T. brucei* ATP synthase subunits (α, β, p18, OSCP, Tb1 and Tb2). The amount of antibody included in this incubation depends on the abundance of the antigen, along with the specificity and sensitivity of the antibody. Based on prior experience in the lab, the following dilutions were used (α – 1:100, β – 1:5000, p18 – 1:2000, OSCP – 1:2000, Tb1 –

1:2000 and Tb2 -1:2000). To wash away unspecifically bound antibodies, the membrane was quickly rinsed with PBS-T, washed once for 15 min and then washed three additional times for 5 min with PBS-T. The blot was then rotated for 1 hour in a 5 ml blocking solution containing the horseradish peroxidase (HRP)-conjugated goat anti-rabbit secondary antibody diluted 1:2000. The previous washing regiment was repeated again. HRP catalyzes the oxidation of luminol in the presence of hydrogen peroxide, a reaction that emits detectable chemiluminescence as a byproduct. Using the ECL Western Blotting Substrate (Bio-Rad), the luminol solution and hydrogen peroxide solution were mixed 1:1. 500 µl of this reagent were applied to the membrane. After a 1 min incubation, chemiluminescence was detected using the ChemiDoc™.

To determine the relative amount of each of these ATP synthase subunits throughout the RNAi induction of a clonal cell line, we needed to include a loading control for each sample. For this purpose, we repeated the above probing procedure with the monoclonal mouse antibody raised against the abundant mitochondrial heat shock protein of 70 kDa (mtHSP70). This antibody was diluted 1:2000. This time the secondary antibody was an HRP-conjugated goat anti-mouse antibody diluted 1:2000. mtHSP70 is a housekeeping gene that remains largely unchanged under most cellular manipulations. Using the Image Lab software (BioRad), the signal intensity from mtHSP70 was used to normalize the signal from each ATP synthase band. From the normalized data the relative intensity of each band was calculated.

## 2.6 Blue Native western blot analyses

### 2.6.1 Induction of cultures, hypotonic lysis and DNA degradation

To determine if a specific *T. brucei* $F_o$ ATP synthase subunit was involved in the dimerization of the complex, we performed a phenotypic screen that would analyze if the depletion of that subunit would preferentially destabilize the dimers of this large multiprotein complex. Therefore, we resolved protein complexes under native conditions and then probed with antibodies that would visualize each conformation of the enzyme ($F_1$ domain, $F_oF_1$ monomers and dimers).

To increase the resolution of the native gel electrophoresis, we reduce the complexity of the protein samples by first enriching our samples for mitochondrial proteins. To achieve this, we performed a hypotonic lysis of the parasites, which results when the cells are swollen in a hypotonic solution and then forced through a small space. This allows us to retain intact organelles while removing the cytosol, which contains almost 85% of all proteins. The RNAi

clonal cell lines used for the previous studies were again induced with tetracycline as described previously. After 0, 2 and 4 days of RNAi induction, $3x10^8$ cells were harvested by centrifugation (1300 x g, 10 min, 4 °C). The cell pellet was resuspended in 1.5 ml ice-cold NET (0.15 M NaCl, 0.1 M EDTA, 10 mM Tris-HCl pH 8.0) and then centrifuged under the same conditions. The cell pellet was resuspended in 1.5 ml hypotonic DTE solution (1 mM EDTA, 1 mM Tris-HCl pH 8.0). The low salt concentration of this solution forced the parasites to intake water. The swollen cells were then disrupted by passing them through a 25 gauge needle three times. Immediately afterwards, 180 µl of 60% sucrose were added to return the tonicity to physiological values, preventing the mitochondria from also bursting. The soluble cytosolic content was then removed by centrifugation (15,000 x g, 10 min, 4 °C). The resulting organellar pellet was resuspended in 500 µl STM (250 mM sucrose, 2 mM $MgCl_2$, 20 mM Tris pH 8.0). To degrade the genomic DNA and decrease the viscosity of the suspension, the sample was treated with 0.7 µl DNase I (Alchimica, cat. # A37780010) in the presence of the following cations: 1.5 µl 1 M $MgCl_2$ and 1.5 µl 0.1 M $CaCl_2$. The reactions were incubated on ice for 1 hour. The DNase treatment was stopped by adding 500 µl ice-cold STE (250 mM sucrose, 10 mM EDTA, 20 mM Tris pH 8.0), which chelates the cations required for enzymatic activity. The remaining soluble DNA fragments were removed by centrifugation (15,000 x g, 10 min, 4 °C). The organellar pellet was washed with 500 µl of STE and centrifuged again (15,000 x g, 10 min, 4 °C). The remaining pellet was stored at -80 °C.

### 2.6.2 Mitochondrial lysis

The mitochondria enriched samples were resuspended in 67 µl of solubilization buffer A (Table 14) and then lysed with the addition of 17 µl 10% dedecylmaltoside (Wittig et al., 2006). After 1 hour incubation on ice, the lysed material was spun in a centrifuge (16,000 x g, 30 min, 4 °C). The supernatant containing soluble proteins along with the solubilized membrane proteins was extracted and transferred to a new tube.

**Table 14: Recipe for 10 ml Solubilization buffer A**. pH adjusted to 7.0 with HCl.

| Reagent | Stock/FW | Amount | Final conc. |
|---|---|---|---|
| NaCl | 1 M | 500 µl | 50 mM |
| Bis-Tris/HCl, pH 7.0 | 1 M | 500 µl | 50 mM |
| Aminocaproic acid | 2 M | 10 µl | 2 mM |
| EDTA | 0.5 M | 20 µl | 1 mM |
| MilliQ | | fill up to 10 ml | |
| Protease Inhibitor (Thermo Scientific, cat. # A32963) | | 1 tablet | |

### 2.6.3 BCA assay

As one type of loading control, we wanted to ensure that approximately the same amount of total protein from each mitochondrial lysis was loaded on the gel. Therefore, the protein concentration from these samples was estimated by the Pierce™ BCA Protein Assay Kit (Thermo Scientific, cat. # 23225). It uses the characteristic of $Cu^{2+}$ cations to be reduced when forming complexes with nitrogen atoms that are parts of peptide bonds. The resulting $Cu^{1+}$ ion forms a purple-colored product by chelation with bicinchoninic acid, which is detected by photometry at 562 nm. BSA standards were prepared in solubilization buffer A and lysed mitochondrial samples were diluted 1:10 (6 µl sample + 54 µl solubilization buffer A) and 1:20 (3 µl sample + 57 µl solubilization buffer A). 25 µl of each sample and standard were pipetted into microplate wells in duplicates before 200 µl of the working reagent (50:1 mix of Reagent A:B) were added. After a 30 min incubation at 37 °C, the absorbance at 562 nm was measured on the Tecan Infinite M200. The equation for a best fit line of the absorbance values measured for the BSA standards was then used to calculate the concentrations of the diluted mitochondrial protein samples.

### 2.6.4 Native PAGE

For Blue Native Western blots it is essential that protein samples are resolved under native conditions so that multiprotein complexes can remain assembled. Therefore, denaturing and reducing agents are avoided while the pH should remain close to physiological values. For these reasons, we used precast NativePAGE™ 3-12% Bis-Tris Protein Gels (Invitrogen, cat. # BN1001BOX). The gel was inserted into a Mini Gel Tank apparatus (Invitrogen, cat. # A25977), the front chamber was filled with cold cathode buffer (50 mM Tricine, 0.002% Coomassie Brilliant Blue (CBB) G-250, 15 mM BisTris, pH 7) and the back chamber with cold anode buffer (50 mM Tricine). To orientate ourselves on the gel and accurately identify the various *T. brucei* ATP synthase complexes, the first lane of each gel was loaded with 10 µl of the NativeMark™ Unstained Protein Standard (Invitrogen, cat. # LC0725). For each of the mitochondrial protein samples, a 20 µl aliquot containing 4 µg of total protein mixed with 2 µl 50% glycerol, 1.5 µl loading dye (0.5 M Aminocaproic acid and 5% CBB G-250) and solubilization buffer A was loaded onto the gel. The gel was run at 100-140 V at 4 °C until the CBB dye front reached the bottom of the gel (2-3 hours). A portion of the mitochondrial lysate (4 µg) was transferred to a new tube and mixed with 3x SDS-PAGE loading dye. These

samples were boiled and then stored at -20 °C until they could be resolved by SDS-PAGE and probed with the mtHSP70 antibody as described previously (section 2.5.4). This signal then served as another loading control for the results detected by Blue Native Western blot analyses.

### 2.6.5 Coomassie staining of MW markers

To visualize the protein standards loaded on the native gels, that first lane of native proteins had to be excised from the gel and incubated in a CBB fixing solution (Table 15) for 10 min on an orbital shaker. The protein ladder was then incubated in a CBB staining solution (Table 16) for 30 min, also on an orbital shaker. Finally, the gel was incubated in a destaining solution (Table 17) overnight on the orbital shaker. A picture of the coomassie stained protein ladder was taken with the ChemiDoc™ using a white light conversion screen.

**Table 15: Recipe for 1 l of CBB fixing solution.**

| Reagent | Stock/FW | Amount | Final conc. |
|---|---|---|---|
| Methanol | 99.9% | 500 ml | 50% |
| Acetic Acid | 99% | 100 ml | 10% |
| MilliQ | | 400 ml | |

**Table 16: Recipe for 400 ml of CBB staining solution.**

| Reagent | Stock/FW | Amount | Final conc. |
|---|---|---|---|
| Methanol | 99.9% | 200 ml | 50% |
| Coomassie Brilliant Blue R250 | | 1.0 g | 0.25% |
| Acetic Acid | 99% | 40 ml | 10% |
| MilliQ | | fill up to 400 ml | |

**Table 17: Recipe for 1 l of CBB destaining solution.**

| Reagent | Stock/FW | Amount | Final conc. |
|---|---|---|---|
| Methanol | 99.9% | 50 ml | 5% |
| Acetic Acid | 99% | 70 ml | 7% |
| MilliQ | | 880 ml | |

### 2.6.6 Electroblotting and probing with antibodies

The transfer sandwich was assembled as described in 2.5.3. However, due to the large size of the native complexes, the proteins were transferred by electroblotting at 100 V for 2 hours at 4 °C. The transfer apparatus was also placed on a stirrer so that the ions in the transfer buffer wouldn't accumulate at the anode and cathode. The antibody probing and

imaging procedures were the same as described in 2.5.4 and were performed with primary antibodies recognizing two subunits of the ATP synthase $F_1$ domain (β, p18) and several $F_o$ subunits (Tb1, Tb2; + OSCP for Tb9). Each of these primary antibodies was diluted 1:1000, while the secondary HRP-conjugated goat anti-rabbit antibodies were diluted 1:2000.

## 2.7 ATP production assay

### 2.7.1 Principle

An ATP production assay is an *in vitro* assay that can measure the amount of ATP generated from isolated mitochondria either by oxidative phosphorylation (OxPhos) or substrate phosphorylation (SubPhos). The assay depends on supplying the mitochondria with ADP and a metabolite that is known to generate ATP either through OxPhos (glycerol-3-phosphate) or SubPhos (α-ketoglutarate). To verify that these substrates have been shuttled through their appropriate metabolic pathways, specific inhibitors are also included. Examples of inhibitors that will block the production of ATP from OxPhos include KCN, which inhibits respiratory complex IV and decreases the mitochondrial membrane potential, and carboxyatractyloside, an inhibitor of the mitochondrial ADP/ATP carrier that supplies the ATP synthase with substrate. The relative amount of ATP produced is then estimated by the addition of luciferase, which catalyzes ATP and D-luciferin to produce bioluminescence. Therefore, the amount of bioluminescence measured on the Orion II luminometer is directly proportional to the amount of ATP produced in the assay. We would like to utilize this assay to determine if ATP synthase monomers can generate ATP as efficiently as dimers of the enzyme.

### 2.7.2 Cell lysis by digitonin

First, a quick and crude PF *T. brucei* mitochondrial preparation was performed by lysing the cell membrane with digitonin, followed by a differential centrifugation step. $1x10^8$ PF *T. brucei* cells that were RNAi induced for either 0, 2 or 4 days were harvested by centrifugation (1300 x g, 10 min, 4 °C). The cell pellet was washed in PBS and resuspended in 500 µl SoTE buffer (Table 18). Next, 500 µl of SoTE buffer containing 0.03% digitonin were added and the tube was inverted one time before being placed on ice for 5 min. The soluble cytosolic content was removed by centrifugation and the mitochondrial enriched pellet was resuspended in 500 µl ATP production assay buffer (Table 19).

**Table 18: Recipe for 100 ml of SoTE buffer.**

| Reagent | Stock/FW | Amount | Final conc. |
|---|---|---|---|
| Tris-HCl, pH 7.75 | 1 M | 2 ml | 20 mM |
| EDTA, pH 8.0 | 0.5 M | 400 µl | 2 mM |
| D-Sorbitol | 182.17 g/mol | 10.93 g | 0.6 M |
| MilliQ | | fill up to 100 ml | |

**Table 19: Recipe for 100 ml of ATP production assay buffer.**

| Reagent | Stock/FW | Amount | Final conc. |
|---|---|---|---|
| Tris-HCl, pH 7.4 | 1 M | 2 ml | 20 mM |
| $KH_2PO_4/K_2HPO_4$ Buffer, pH 7.4 | 100 mM | 15 ml | 15 mM |
| $MgSO_4$ | 1 M | 15 ml | 15 mM |
| Sorbitol | 182.17 g/mol | 10.93 g | 0.6 M |
| BSA, fatty acid free | | 250 mg | 2.5 mg/ml |
| MilliQ | | fill up to 100 ml | |

### 2.7.3 Reaction setup

For each reaction, 75 µl of mitochondrial enriched material were mixed with the ATP production assay buffer such that the total reaction volume would be 84 µl. Where applicable, 2 µl of 1.8 mM ADP, 210 mM glycerol-3-phosphate (substrate for OxPhos + some background ATP production, including SubPhos), 42 mM KCN (inhibitor of complex IV) and/or 273 µM carboxyatractyloside (inhibitor of ADP/ATP carrier protein) were added. The reaction setup for each harvested culture was as follows:

1. Buffer only (negative control)
2. ADP (negative control)
3. Glycerol-3-phosphate (blank)
4. Glycerol-3-phosphate + ADP (OxPhos + background ATP prod.)
5. Glycerol-3-phosphate + ADP + KCN (background ATP prod.)
6. Glycerol-3-phosphate + ADP + Carboxyatractyloside (background ATP prod.)

After exactly 30 min incubation, 1.5 µl of 70% perchloric acid were added to stop the reaction by precipitating all proteins. The samples were incubated for 10 min and centrifuged (15,000 x g, 5 min, 4 °C). 60 µl of the supernatant were transferred to a new tube and 11.5 µl of 1 M KOH were added to neutralize the perchloric acid. The sample was then incubated for 10 min and centrifuged (15,000 x g, 5 min, 4 °C). The resulting supernatant contained the ATP we wanted to measure. 10 µl of this sample were combined with 40 µl of 0.5 M Tris-Acetate

(pH 7.75) in the well of a 96-well bioluminescence plate. After the 50 µl injection of the luciferase reagent (Roche), bioluminescence was measured on the Orion II Microplate Luminometer (Berthold Technologies). To estimate the amount of ATP generated by OxPhos, the bioluminescence values from reactions 5 and 6 were compared to the values obtained from reaction 4.

# 3 Results

## 3.1 Molecular cloning

### 3.1.1 PCR amplicons

To generate PF *T. brucei* regulatable RNAi cell lines, we needed to create plasmids containing gene specific sequences. This process of molecular cloning began with PCR to amplify the selected region of each respective gene (Tb12, Tb13 and Tb14) that would be inserted into the pAZ055 RNAi plasmid. To determine if the PCR reaction was successful, the resulting amplicons were resolved by electrophoresis on an agarose gel and then visualized with ethidium bromide staining. A representative image (Figure 7) from these gels indicates that the PCR produced a single intense band of the predicted size. To isolate the amplicon from any potential primer dimers or unspecific amplification products of various lengths, the bands were cut from the gel and the DNA extracted.

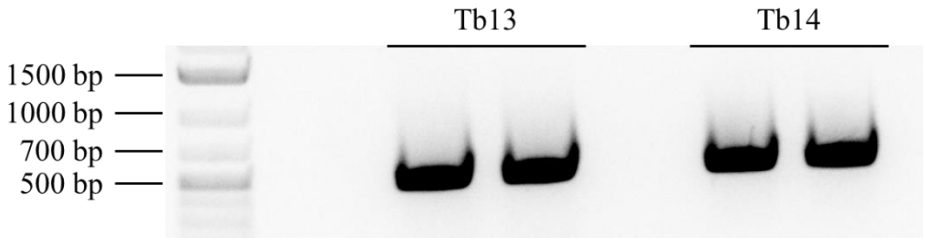


**Figure 7: Representative DNA bands of undigested PCR products.** 50 µl PCR amplicons of ATPaseTb13 (478 bp) and Tb14 (471 bp) were run on a 1% agarose gel after addition of 6 µl 10x DNA loading dye.

### 3.1.2 Generation of the intermediate pAZ055 RNAi MCS1 plasmids

Restriction digests (KpnI, BamHI) were performed for the PCR products, as well as for 9 µg of the pAZ055 plasmid. While the digested PCR amplicons could be cleaned up on a spin column, the linearized pAZ055 plasmid was resolved on a 1% agarose gel. In each case, the expected band appeared around 5050 bp (Figure 8). The lighter bands above and below indicate that the digestion was incomplete, meaning that some of the intact circular plasmids remained in the solution. This would be problematic in the downstream transformations because this uncut plasmid would preferentially be absorbed, leading to numerous colonies on the transformation plate that contained the plasmid without any insert. To reduce this outcome, it was required to gel extract the digested pAZ055 plasmid. The digested amplicons and pAZ055 plasmid were then ligated into new recombinant DNA molecules.

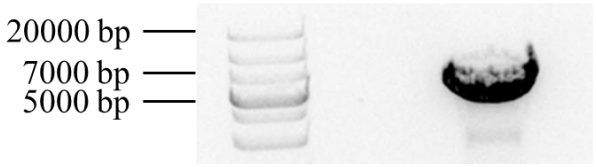


**Figure 8: Restriction digest of pAZ055 plasmid (KpnI, BamHI).** 9 µg total plasmid DNA were run on a 1% agarose gel after a 2 hour restriction digest. UV exposure shows a linearized plasmid band at 5067 bp, also visible are contaminating bands of the undigested plasmid in the nicked-circular and supercoiled conformations.

After ligation, the recombined plasmids (including a negative control without the PCR amplicon) were transformed into competent XL-1 blue *E. coli* cells, which were then plated on agar plates. The number of bacterial colonies on the positive plates was always plentiful, while the plate with the negative control ranged between none and slightly less than on the positive plate. If the negative plate had very few colonies, it signified that the gel extraction of the digested pAZ055 contained very few uncut DNA molecules. Therefore, it was interpreted that most of the colonies present on the corresponding positive plate successfully contained the pAZ055 plasmid with the specific *T. brucei* RNAi amplicon inserted. However, if the negative plate had almost as many colonies as the positive plate, it was assumed that the pAZ055 digest was incomplete and remaining circular plasmids contaminated the transformation event. Thus, more of the colonies on the corresponding positive plate would need to be screened. Depending on these results from the negative plate, 2-8 colonies from the positive plate were selected for plasmid isolation. 1 µg of each plasmid was then analyzed by restriction digest and gel electrophoresis. In a representative case (Figure 9), the negative control contained only a few colonies and all of the isolated plasmids were proven to contain the RNAi insert, which was represented by a single band appearing at the respective size (400-600 bp). All the plasmid DNA clones were tested positive for the insert in this representation.

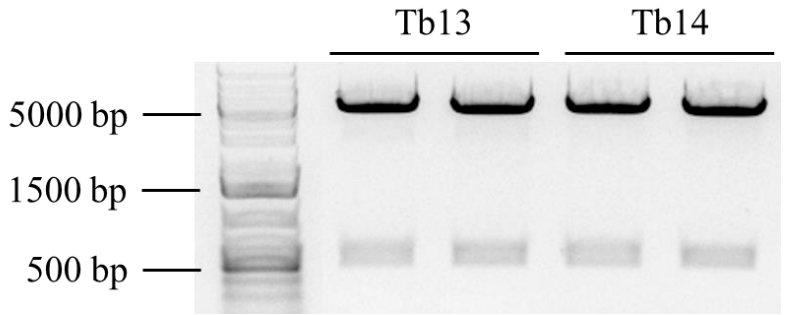


**Figure 9: Representative DNA bands of MCS1 plasmid restriction digest analyses.** Plasmids generated from the ligation of the RNAi amplicon into the first multiple cloning site were isolated from various bacterial colonies and digested with the restriction enzymes KpnI and BamHI. Linearized parental plasmid DNA is visible at ~5000 bp, while the inserts appear at their respective sizes (400-600 bp).

### 3.1.3 Generation of the final pAZ055 RNAi plasmids

A single DNA clone for each RNAi plasmid was selected to incorporate the gene specific amplicon into MCS2. The required cloning steps were performed as outlined above, with both the RNAi amplicons and the pAZ055 RNAi MCS1 plasmids digested with XbaI and XhoI. The linearized plasmids resolved on agarose gels again revealed an intense band at the expected size, as well as minor contaminating bands of undigested plasmid (Figure 10).

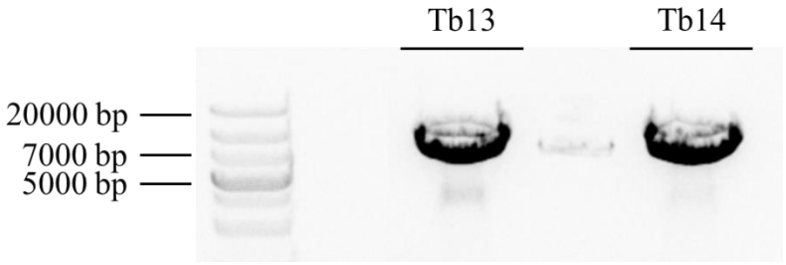


**Figure 10: Representative DNA bands of digested plasmid containing the PCR amplicon in the first cloning site.** 10 µg of the intermediary plasmids for Tb13 (5508 bp) and Tb14 (5501 bp) pAZ055 RNAi were incubated for 2 hours with restriction enzymes XbaI and XhoI, then run on a 1% agarose gel for 60 min. Intense bands of the expected size of the linearized plasmids (Tb13 - 5508 bp and Tb14 - 5501 bp) were visualized by ethidium bromide staining.

The pAZ055 RNAi plasmids were isolated from bacterial colonies transformed with the recombinant DNA ligated with the RNAi amplicon at MCS2. These plasmids were then independently digested with both pairs of restriction enzymes (KpnI & BamHI, XhoI & XbaI) to verify if the completed RNAi plasmid contained the gene specific RNAi amplicon at both MCS1 and MCS2. A representative gel of digested Tb13 and Tb14 RNAi plasmids (Figure 11) indicates that both multiple cloning sites contain an insert of the expected size (400-600 bp).

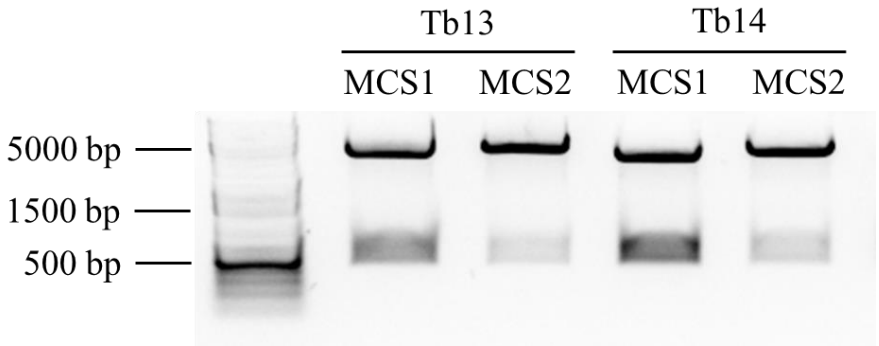


**Figure 11: Representative restriction digest analyses of completed pAZ055 RNAi plasmids.** Finalized RNAi plasmids of Tb13 and Tb14 were isolated and digested with both sets of restriction enzymes (KpnI and BamHI for MCS1, XhoI and XbaI for MCS2). Linearized plasmid DNA is visible at ~5500 bp, while inserts appear at their respective sizes (400-600 bp).

### 3.1.4 Sequencing

A single DNA clone of each successful *T. brucei* RNAi plasmid generated was chosen for sequencing to ensure that both RNAi inserts contained no significant coding errors and that they were in the correct orientation. Pairwise alignment of the sequenced Tb12 RNAi cloning sites with the *in silico* generated sequence (Figure 12) revealed two major insertion mutations, presumably caused by slippage of the DNA polymerase in highly repetitive regions. Attempts to repeat the cloning procedure with a polymerase exhibiting 3'→5' exonuclease proofreading activity were unsuccessful. Since the mutations were not consecutive and RNAi can handle some limited amount of mismatches, we presumed that the RNAi efficiency would not be significantly reduced by this unavoidable consequence. Alignment of the Tb13 RNAi cloning sites (Figure 13) revealed a single point mutation inside the coding region (MCS1), which is negligible for RNAi. The alignment of the Tb14 RNAi construct (Figure 14) revealed no errors within the cloned region.

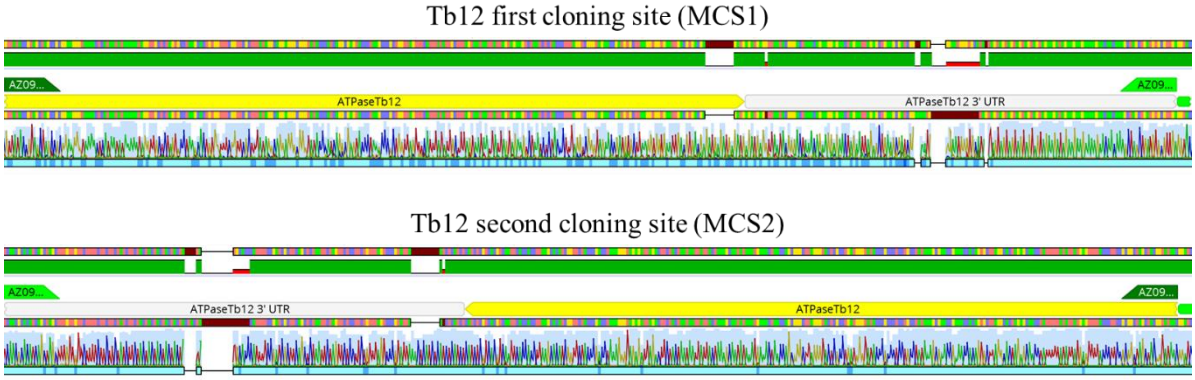


**Figure 12: Geneious alignment of sequenced Tb12 RNAi plasmid with *in silico* generated sequences of both cloning regions.** The alignment reveals two major ambiguities in highly repetitive regions of the ATPaseTb12 amplicon for both cloning sites (top and bottom alignments). The solid green bars indicate identical nucleotides, whereas gaps in the green bar represent mismatched nucleotides resulting from an insertion event. Software: Geneious 11.1 (https://www.geneious.com).

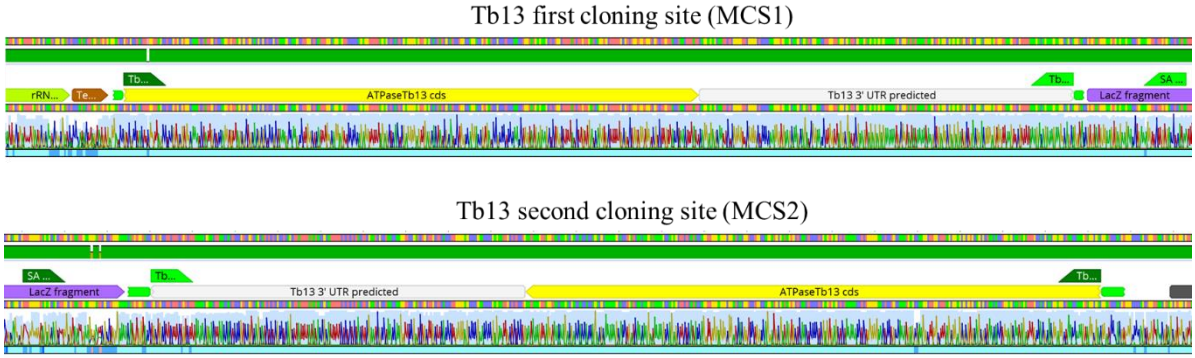


**Figure 13: Geneious alignment of sequenced Tb13 RNAi plasmid with *in silico* generated sequences of both cloning regions.** The sequences are almost 100% homologous with the exception of one single nucleotide replication error near the 5' end of the ATPaseTb13 coding region inserted to the first cloning site (top alignment). Software: Geneious 11.1 (https://www.geneious.com).

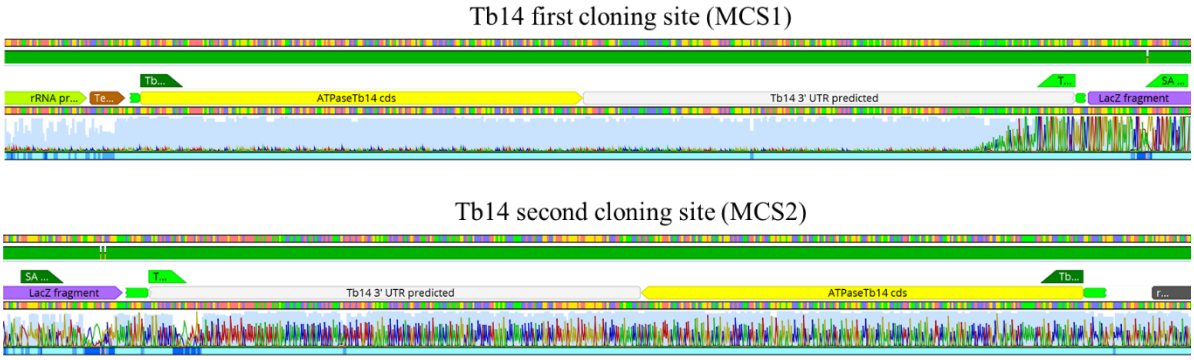


**Figure 14: Geneious alignment of sequenced Tb14 RNAi plasmid with *in silico* generated sequences of both cloning regions.** The sequences are 100% homologous within the two cloning sites. Software: Geneious 11.1 (https://www.geneious.com).

## 3.2 Growth curves

While it is known that ATP synthase enzymes form dimers that are assembled into rows that affect cristae shape in mitochondria, it is less well understood if the these dimers are essential for the organism. Therefore, we first characterized the importance of each $F_o$ subunit by comparing the growth of RNAi induced and non-induced cultures from the generated Tb12, Tb13, and Tb14 cell lines. Also included in our studies was a cell line generated by another member of the lab, which was designated Tb9 RNAi. The cells were grown in 10 ml media containing SDM-79, which is a glucose-rich medium. The growth curves were performed on three clones of each potential dimerization subunit. To simplify the interpretation of the data, we have included the data from just a single clone that best represents the group of cell lines analyzed (Figure 15). The experiment indicates that the effects of RNAi induction are similar for Tb12, Tb13 and Tb14, with a significant growth phenotype first detected on day three of tetracycline induction. The average doubling times were calculated from this data and revealed similar trends between the three RNAi cell lines, with the doubling time increasing from 13-15 hours in the non-induced cultures to 17-22 hours for the induced cultures. Interestingly, the Tb9 knockdown had a less pronounced effect with the average doubling time increasing only from 14-15 hours to 16-17 hours. This slight growth phenotype first manifested after four days of RNAi induction. This difference could either indicate that the RNAi depletion of Tb9 was less efficient than for the other subunits, or the function of Tb9 was different from the others.

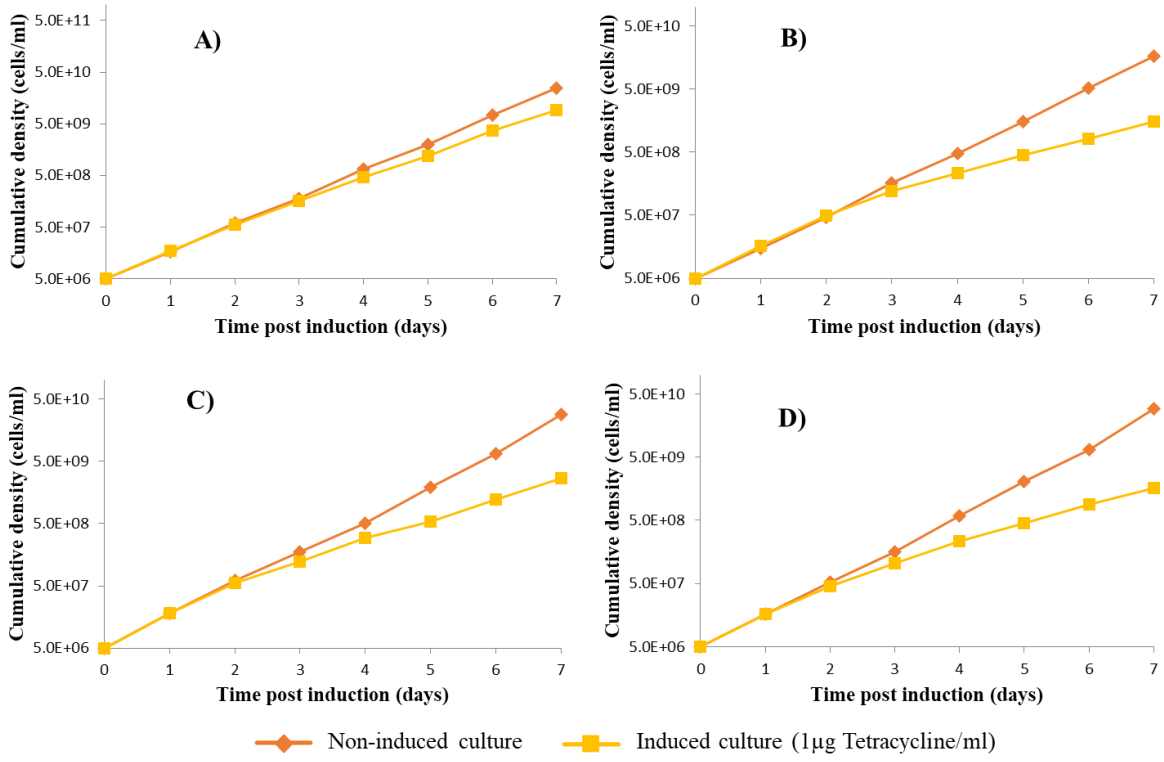


**Figure 15: Cumulative growth curves of selected clones.** Knockdown of ATPase subunits (A) Tb9, (B) Tb12, (C) Tb13 and (D) Tb14 by RNAi induction. The growth of cultures either continually treated with tetracycline or not was monitored for 7 consecutive days. While significant growth defects were observed for Tb12, Tb13 and Tb14, these effects were limited for the Tb9 RNAi induction.

## 3.3 qPCR

The RNAi efficiency to deplete a targeted gene product was analyzed by qPCR for the selected clones of Tb12, Tb13 and Tb14 RNAi regulatable cultures (unfortunately, the Tb9 RNAi efficiency was not included in this study). We measured the relative abundance of a specific transcript by comparing the data from samples induced for 2 (IND2) or 4 (IND4) days with non-induced samples. These values were normalized to two internal reference housekeeping genes (18S rRNA and β-tubulin). The ratio of induced/non-induced abundance was then calculated for each induction time point and reference gene separately (Figure 16). These results indicate that each of the targeted transcripts were significantly depleted in all induced cultures, even at the time point harvested immediately before the growth phenotype was observed (IND2). The accuracy of the assay is reinforced by the insignificant change in the depletion of the targeted transcript observed between the different reference genes.

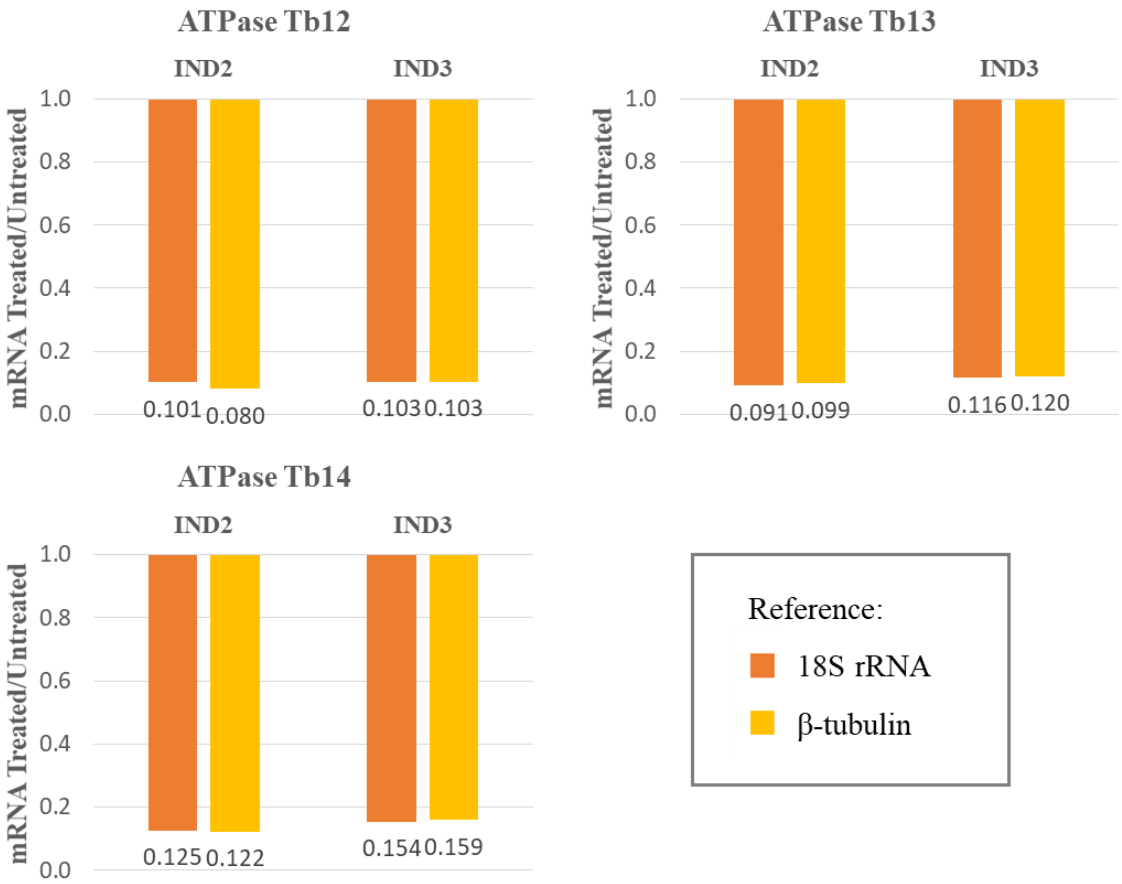


**Figure 16: Determining levels of RNAi efficiency by qPCR.** The mRNA abundance of respective ATPase subunits in induced cultures was compared to untreated cultures, both standardized by simultaneous measurement of two internal reference housekeeping genes. In all samples, the targeted transcript was significantly depleted.

## 3.4 Steady state western blot analyses

Ideally, to study the importance of ATP synthase dimers, the depletion of a subunit at the dimer interface would primarily disrupt dimers but not the monomers of the complex. However, if an $F_o$ subunit at the dimer interface has an additional structural role, it will most likely also destabilize the monomer. Due to the assembly process of this multiprotein complex, this disruption of the monomeric structure would strongly affect the protein levels of the peripheral stalk and supernumerary subunits, while having a minimal negative effect on the $F_1$ subunits (He et al., 2018). In fact, the depletion of $F_o$ subunits often leads to the accumulation of the stable catalytic $F_1$ moiety (Šubrtová et al., 2015). To analyze how the loss of a potential dimerization subunit effects the protein expression levels of various $F_oF_1$-ATP synthase subunits during the progression of Tb9, Tb12, Tb13 and Tb14 RNAi silencing, we combined SDS-PAGE with the immunostaining of specific antibodies that recognize the ATP synthase subunits α, β, p18, OSCP, Tb1 and Tb2. The relative amount of these subunits can be used to infer monomer and subcomplex stability as the unsuccessful incorporation of subunits into an

assembled monomeric complex or subcomplex are more susceptible to degradation by proteinases. The obvious caveat about this observation from previous experiments in the lab is that we do not know much about the half-life of these individual subunits, especially the membrane embedded $F_o$ subunits.

In the case of Tb9 knockdown (Figure 17), normalization data suggests that the concentration of $F_1$ subunits does not change significantly after RNAi induction. However, the abundance of Tb1 and Tb2 appear to decrease slightly, while OSCP levels increase slightly. This discrepancy between the $F_o$ subunits is supported by ongoing work in the lab indicating that *T. brucei* OSCP typically acts in a manner that is more similar to $F_1$ subunits than other $F_o$ components.

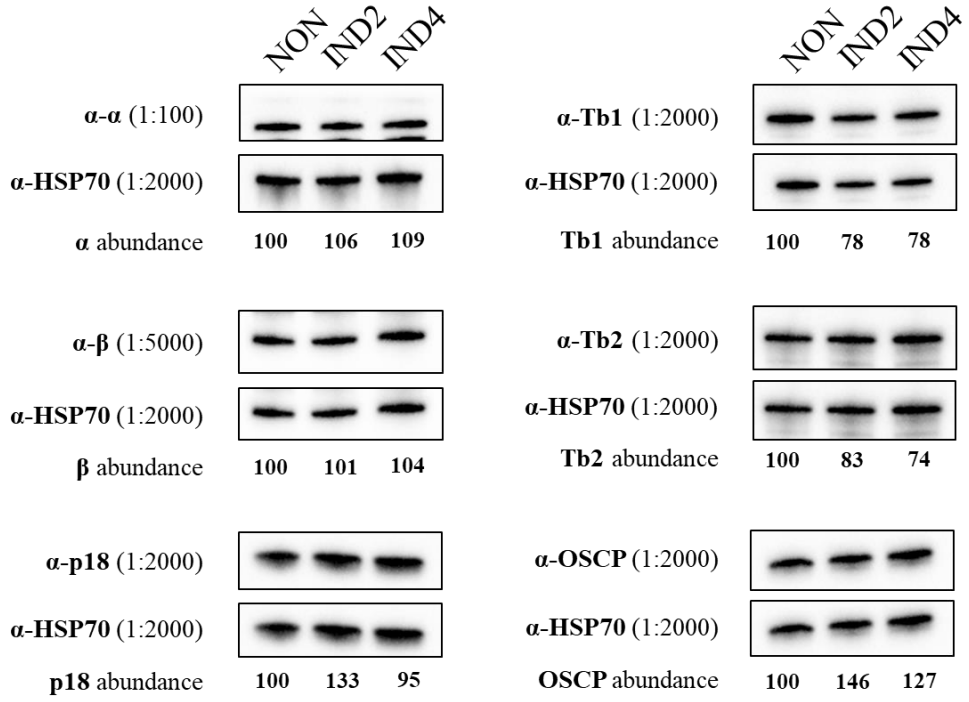


**Figure 17: Steady state western blots of ATPaseTb9 RNAi cell cultures after 0 (NON), 2 (IND2) and 4 (IND4) days of induction.** PVDF membranes were probed with a total of 6 antibodies recognizing previously identified ATP synthase subunits (at indicated dilutions). The blots were also probed with the anti-HSP70 antibody, which serves as a loading control to normalize the changes observed in the ATP synthase band intensities. Normalized intensities are given as percentage of the non-induced sample.

The steady state levels of ATP synthase subunits in the Tb12 RNAi cell line (Figure 18) differs significantly from Tb9. The $F_1$ subunits, especially p18, increase in concentration, while the $F_o$ subunits Tb1 and Tb2 are significantly diminished. Unlike the other $F_o$ subunits, OSCP expression levels are slightly increased.

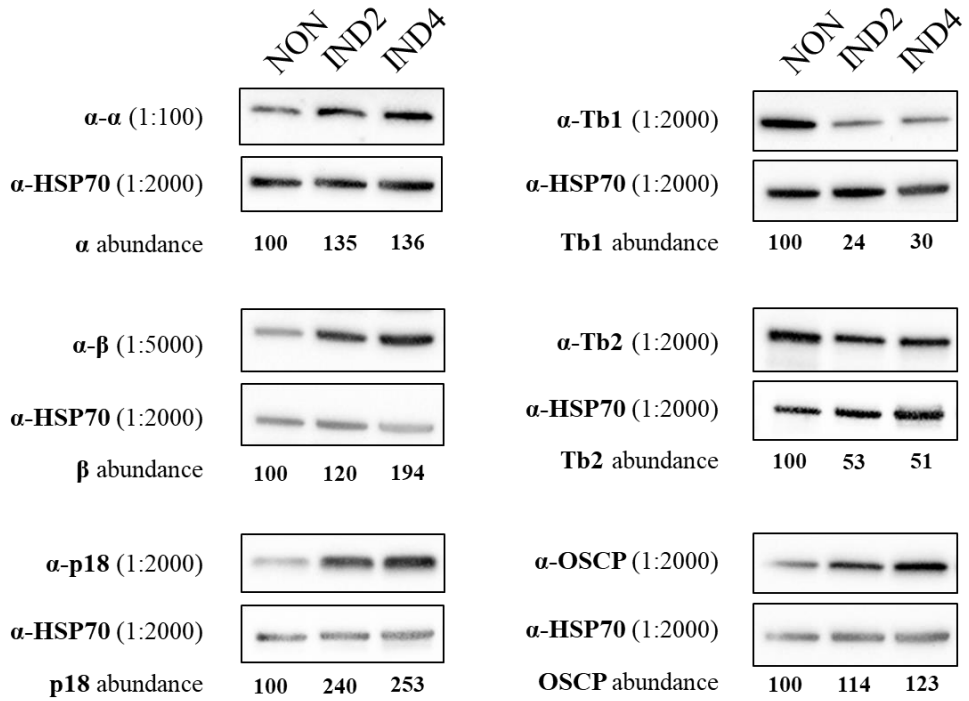


**Figure 18: Steady state western blots of ATPaseTb12 RNAi cell cultures after 0, 2 and 4 days of induction.** PVDF membranes were probed with a total of 6 antibodies recognizing previously identified ATP synthase subunits (at indicated dilutions). The blots were also probed with the anti-HSP70 antibody, which serves as a loading control to normalize the changes observed in the ATP synthase band intensities. Normalized intensities are given as percentage of the non-induced sample.

The expression patterns for ATP synthase in the Tb13 RNAi cell line are similar to those observed for the Tb12 knockdown (Figure 19). The levels of $F_1$ subunits increase, whereas OSCP expression changes insignificantly. The abundance of Tb1 and Tb2 again decreases, but not as significantly as for the Tb12 RNAi parasites.

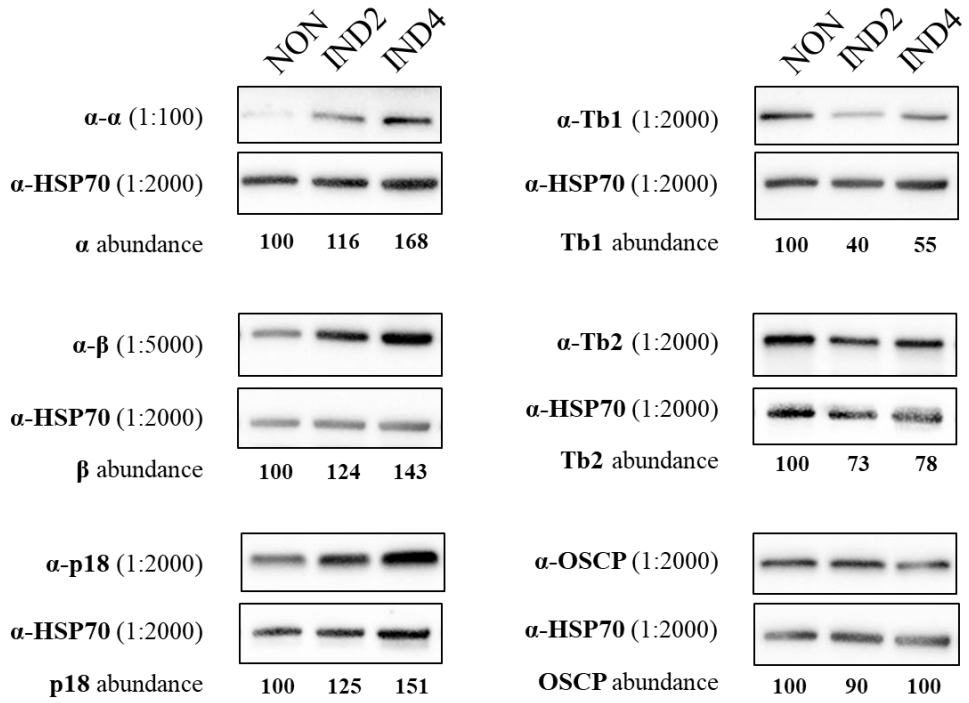


**Figure 19: Steady state western blots of ATPaseTb13 RNAi cell cultures after 0, 2 and 4 days of induction.** PVDF membranes were probed with a total of 6 antibodies recognizing previously identified ATP synthase subunits (at indicated dilutions). The blots were also probed with the anti-HSP70 antibody, which serves as a loading control to normalize the changes observed in the ATP synthase band intensities. Normalized intensities are given as percentage of the non-induced sample.

The Tb14 knockdown produces a more moderate decrease in the expression of Tb1 and Tb2, similar to the Tb13 RNAi cells (Figure 20). The OSCP levels are also largely unaffected, but so are the $F_1$ subunits. In this respect, the Tb14 RNAi cell line reflects the observations made from the Tb9 knockdown.

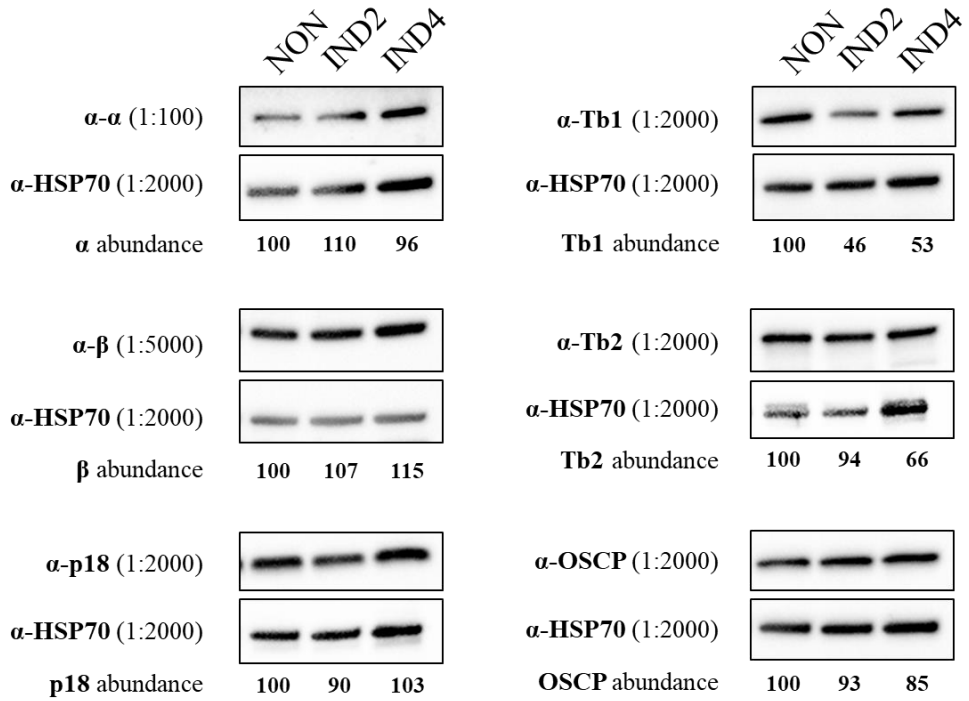


**Figure 20: Steady state western blots of ATPaseTb14 RNAi cell cultures after 0, 2 and 4 days of induction.** PVDF membranes were probed with a total of 6 antibodies recognizing previously identified ATP synthase subunits (at indicated dilutions). The blots were also probed with the anti-HSP70 antibody, which serves as a loading control to normalize the changes observed in the ATP synthase band intensities. Normalized intensities are given as percentage of the non-induced sample.

The abundance of each ATP synthase subunit analyzed by western blot is expressed in Table 20 as a percentage of the amount detected in the respective non-induced RNAi cell lines. While not a precise indicator of monomer stability, several interesting trends can be gleaned from this dataset. Most importantly, the relative lack of change in the individual $F_1$ and $F_o$ subunits examined in the Tb9 RNAi cell line suggests that the depletion of Tb9 does not significantly alter the stability of the monomer complex. This suggests that Tb9 would be a good candidate to further investigate as a subunit involved in ATP synthase dimerization. While there is a moderate effect on the $F_o$ subunits Tb1 and Tb2 in the Tb14 knockdown cells, the $F_1$ subunits and OSCP remain fairly steady in their abundance. While not a perfect phenotype to address detailed questions about the importance of *T. brucei* ATP synthase dimers, it does suggest that the role of Tb14 at the dimer interface should be further explored. Meanwhile, the drastic changes observed in the overall protein abundance for both the Tb12 and Tb13 RNAi cell lines suggests that these $F_o$ subunits play a significant role in the general structure of the enzyme. Finally, in each of the Tb12, Tb13 and Tb14 RNAi cell lines, the abundance of the supernumerary subunit Tb1 is more affected than the peripheral stalk subunit Tb2.

**Table 20: Relative abundance of ATP synthase subunits after 2 and 4 days of RNAi induction.** Displayed numbers are percentages of the amount detected in the non-induced sample.

| | Tb9 | | Tb12 | | Tb13 | | Tb14 | |
|---|---|---|---|---|---|---|---|---|
| | **IND2** | **IND4** | **IND2** | **IND4** | **IND2** | **IND4** | **IND2** | **IND4** |
| **α** | 106 | 109 | 135 | 136 | 116 | 168 | 110 | 96 |
| **β** | 101 | 104 | 120 | 194 | 124 | 143 | 107 | 115 |
| **p18** | 133 | 95 | 240 | 253 | 125 | 151 | 90 | 103 |
| **OCSP** | 146 | 127 | 114 | 123 | 90 | 100 | 93 | 85 |
| **Tb1** | 78 | 78 | 24 | 30 | 40 | 55 | 46 | 53 |
| **Tb2** | 83 | 74 | 53 | 51 | 72 | 78 | 94 | 66 |

## 3.5 Blue Native western blot analyses

To better comprehend if these selected $F_o$ subunits contribute to the interactions between two ATP synthase monomers, we needed to advance beyond protein analyses under denaturing conditions and instead analyze the assembled ATP synthase complex under native conditions. Therefore, we employed Blue Native (BN) western blot analyses to visualize intact ATP synthase complexes that are present under physiological conditions within the *T. brucei* mitochondrion. Since the mitochondrial proteins resolved by gel electrophoresis in this technique were able to maintain their proper folds, protein-protein interactions were stabilized. We then immunostained blots containing these resolved protein complexes with antibodies of 4-5 well-known ATP synthase subunits (β, p18, Tb1, Tb2 and OSCP) in order to visualize complexes and subcomplexes in which these subunits are incorporated. When staining with antibodies that recognize $F_o$-subunits, this commonly reveals two bands. The upper band of 1000-1200 kDa is believed to represent oligomers (including dimers) of ATP synthase, while the lower band of 800-950 kDa represents the monomers. Staining with antibodies that recognize $F_1$-subunits detected these same higher molecular weight complexes, but also revealed two smaller additional bands that occur in close proximity. The lower band is believed to represent $F_1$ alone, whereas the upper band is likely the $F_1$ attached to the c-ring.

BN Western blotting was first performed on material isolated from the ATPaseTb12 RNAi cell line induced for 0, 2 and 4 days with tetracycline (Figure 21). A clear reduction in the concentration of both monomers and oligomers was observed both before the appearance of a growth phenotype (IND2) and after (IND4), independent of which antibody was used for visualization. Additionally, the concentration of $F_1$ subcomplexes seems to remain steady (α-β) or increase slightly (α-p18) after two days of RNAi induction.

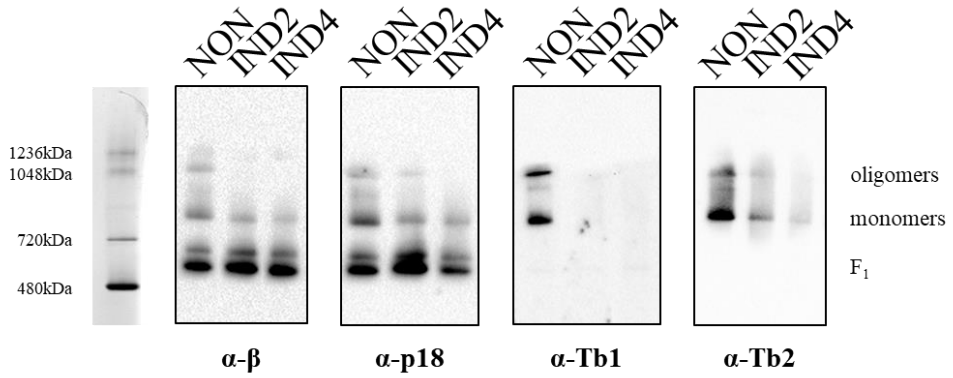


**Figure 21: Blue Native Western blots of ATPaseTb12 RNAi cell cultures after 0 (NON), 2 (IND2) and 4 (IND4) days of tetracycline induction.** PVDF membranes were probed with antibodies recognizing specific subunits of ATP synthase in order to visualize the complexes containing these subunits (monomers, oligomers and $F_1$ subcomplexes). Each primary antibody was added at 1:1000 dilution.

BN western blotting of the Tb13 RNAi cell cultures revealed a similar phenotypic outcome as for Tb12 (Figure 22). Both oligomers and monomers are diminished after RNAi induction, while the $F_1$ subcomplexes accumulate by the second day of Tb13 depletion.

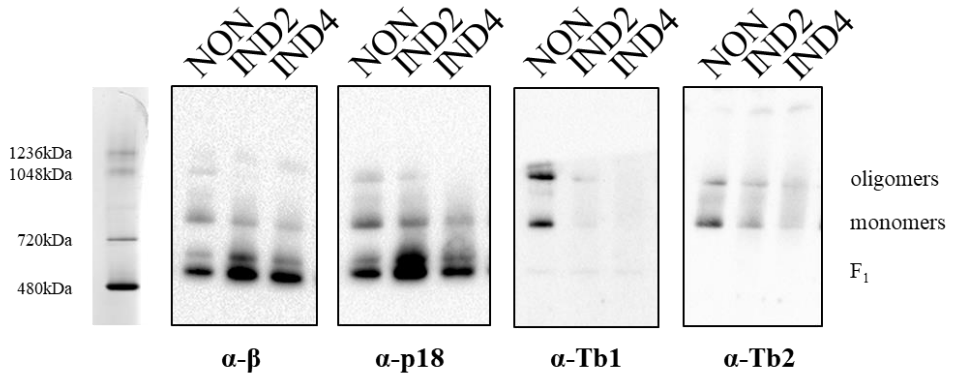


**Figure 22: Blue Native Western blots of ATPaseTb13 RNAi cell cultures after 0, 2 and 4 days of induction.** PVDF membranes were probed with antibodies recognizing specific subunits of ATP synthase in order to visualize the complexes containing these subunits (monomers, oligomers and $F_1$ subcomplexes). Each primary antibody was added at 1:1000 dilution.

The depletion of Tb14 also indicates a reduction in the abundance of monomers and oligomers, as well as a slight increase in the $F_1$ moiety (Figure 23). However, upon closer inspection, it appears that the monomers are not destabilized as much as in the Tb12 and Tb13 RNAi cells. While this would correlate with the steady state protein expression levels we observed in the denaturing western blot analyses for Tb14, exact quantification from BN

Western blots is not very reliable. Therefore, it would be necessary to repeat these analyses before making any bold conclusions.

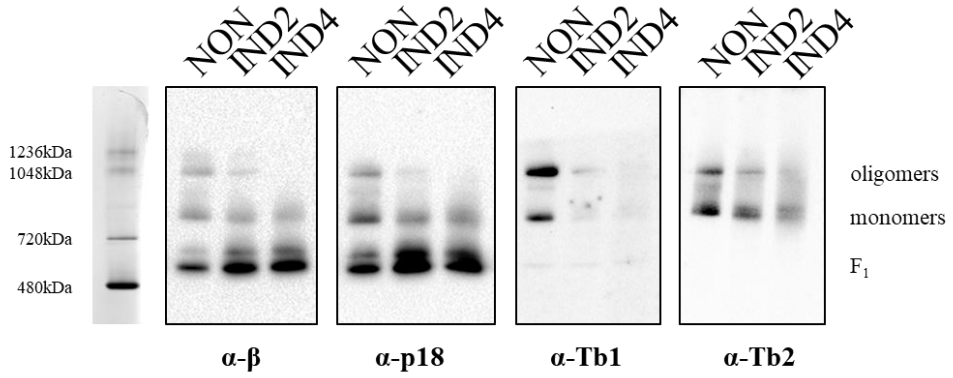


**Figure 23: Blue Native Western blots of ATPaseTb14 RNAi cell cultures after 0, 2 and 4 days of induction.** PVDF membranes were probed with antibodies recognizing specific subunits of ATP synthase in order to visualize the complexes containing these subunits (monomers, oligomers and $F_1$ subcomplexes). Each primary antibody was added at 1:1000 dilution.

Blue Native Blots of the Tb9 RNAi cell cultures (Figure 24) indicates a decrease in the abundance of ATP synthase oligomers, whereas the intensity of the monomeric complexes increases significantly. The amount of the $F_1$ subcomplexes also increases as the monomers become more abundant. Potentially this could indicate that even the detected monomers are inherently unstable on some level. Most importantly, this indicates that Tb9 is a prime candidate to play a significant role in the dimerization of *T. brucei* ATP synthase, while having minimal impacts on the assembly of the monomeric complex.

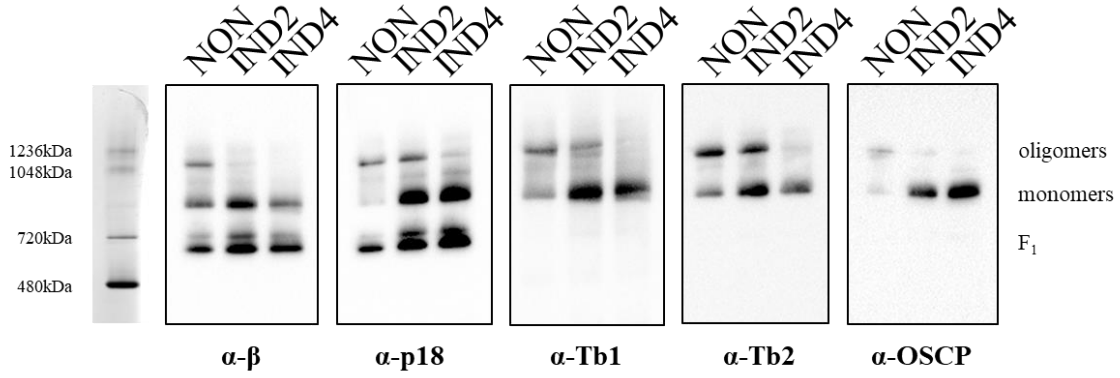


**Figure 24: Blue Native Western blots of ATPaseTb9 RNAi cell lines after 0, 2 and 4 days of induction.** PVDF membranes were probed with antibodies recognizing specific subunits of ATP synthase in order to visualize the complexes containing these subunits (monomers, oligomers and $F_1$ subcomplexes). Each primary antibody was added at 1:1000 dilution.

Despite loading equal amounts of total protein, an aliquot of each lysed mitochondria sample was denatured and resolved by SDS-PAGE and then probed with the mtHSP70 antibody. This served to act as another type of loading control (Figure 25) since the abundance of mtHSP70 should remain largely unchanged in these RNAi cell lines. Normalization data suggests that loading errors did not exceed 16%. Due to the comparatively large differences in the chemiluminescence intensity observed in the BN western blot analyses, these errors should be negligible.

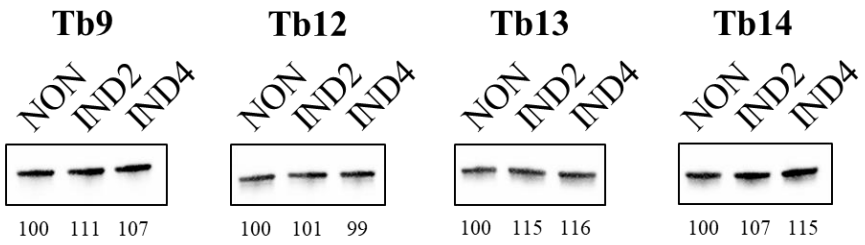


**Figure 25: HSP70 loading control for Blue Native Western blots of Tb9, Tb12, Tb13 and Tb14 RNAi.** Each blot contained samples isolated from RNAi cell lines that were either non-induced (NON) or induced with tetracycline for 2 (IND2) or 4 days (IND4). The abundance of mtHSP70 was normalized as percentage of the non-induced sample.

## 3.6 ATP production assay

Our preliminary results suggest that we can utilize the Tb9 RNAi cell line to generate ATP synthase monomers by the destabilization of the dimer. With this powerful tool, we can now attempt to answer if the dimerization of ATP synthase enhances the efficiency of the enzyme activity compared to the values measured with the monomer. Therefore, we employed an ATP production assay that measures the relative amount of ATP produced by OxPhos in mitochondria isolated from non-induced and induced Tb9 RNAi cultures. Since the Tb12 knockdown cells seem to equally affect ATP synthase monomers and dimers, we used this cell line as control to compare the effects of RNAi induction.

For each time point, the total amount of ATP produced from the OxPhos substrate glycerol-3-phosphate was determined from the measured bioluminescence generated by the addition of luciferase and luciferin. To determine the level of background ATP measured in this assay, identical mitochondrial samples were treated with the inhibitors KCN and Carboxyatractyloside, which should completely block ATP synthesized by OxPhos (Figure 26). The produced ATP generated by OxPhos from the oxidation of glycerol-3-phosphate without the presence of any inhibitor, revealed a reduction in ATP synthase activity by 46% (IND2) and 27% (IND4) when Tb9 RNAi is induced. The background amount of ATP

produced was similar among all samples with a contribution of 17-23% when KCN was used as inhibitor and 28-30% when Carboxyatractyloside was utilized. The measured bioluminescence intensities were generally lower when measuring the samples isolated from the Tb12 RNAi cultures and always lowest for the non-induced sample, including the negative controls and blank. The lower values obtained from the negative control samples suggest that the amount of lysed cell content was unequal, which might be due to an error that occurred during sample preparation. Thus this data sample cannot be properly interpreted. While the decreased ATP production in the Tb9 RNAi cell lines suggests that the ATP synthase monomers are less efficient at producing ATP, these experiments will need to be repeated to include a properly working control (Tb12 RNAi). Only then we will be able to apply some statistical analysis to these results.

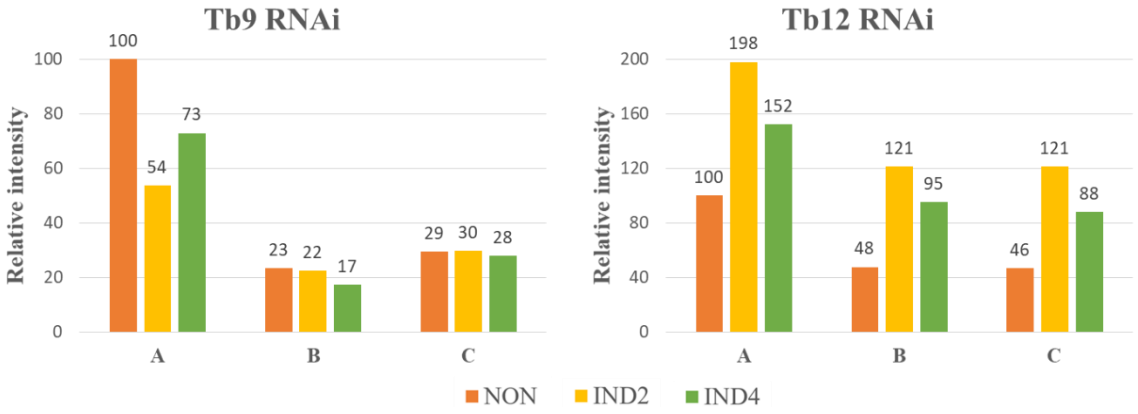


**Figure 26: ATP production assay of RNAi induced cultures under addition of A) Glycerol-3-phosphate, B) Glycerol-3-phosphate and KCN, C) Glycerol-3-phosphate and Carboxyatractyloside.** Bioluminescence intensity was measured after the addition of luciferase and luciferin. Relative intensities are portrayed as percentage in relation to the non-induced sample A of respective cell lines.

# 4 Discussion

Screening of *T. brucei* ATP synthase $F_o$ subunits was performed in order to obtain knowledge about their contributions to the structure and activity of the enzyme. By assuming the existence of at least one subunit primarily involved in dimer formation with only a minor role in monomer stability, we hypothesized that the deletion of such a subunit should induce depletion of dimers, but not monomers. We performed BN Western blotting in order to detect subunits involved in dimerization. Once identified, regulatable RNAi cell lines of these subunits can be used to analyze whether the formation of dimers enhances the enzymatic activity of the complex. Additionally they can be used to examine the effects of dimer depletion on mt ultrastructure since cristae biogenesis largely relies on the self-assembly of ATP synthase dimers into rows (Blum et al., 2019).

Blue Native Western blots of RNAi cell cultures suggest that knockdown of Tb12, Tb13 and Tb14 each affect the complex in a similar way, depleting both monomers and dimers. This suggests that all three subunits are essential for $F_oF_1$ assembly and stability. In contrast, the Tb9 knockdown leads to the depletion of dimers while the amount of monomers increases. This strongly suggests that Tb9 is primarily involved in dimer formation. Since loss of dimers directly causes monomer concentration to increase, it cannot be inferred whether Tb9 is required for monomer stability, although if so, then only to a lower extent than the other subunits. From Blue Native Western blots stained by antibodies of $F_1$ subunits (β and p18), it can be inferred that the $F_1$ subcomplexes also become more abundant, which is commonly seen when the monomeric $F_oF_1$ complex loses stability (as in Tb12, Tb13 and Tb14 knockdown). This might be either because Tb9 is indeed required for monomer stability or related to the circumstance that more $F_oF_1$ complexes are present mainly as monomers rather than dimers, which would suggest that monomers are themselves less stable than dimers, independent of presence of Tb9.

ATPaseTb9 is a Kinetoplasid (class of Euglenozoa) specific subunit and a structural homolog of ATPEG1 in *Euglena*, a related Euglenozoan organism. In *Euglena gracilis*, the dimer interface is formed in three distinct layers by an extension of subunit d (homolog of Tb2), ATPEG1 and ATPEG2 (Mühleip et al., 2019). Preliminary data of the *T. brucei* ATP synthase structure elucidation suggests that Tb9 forms the majority of inter-monomer contacts, though Tb14, which has no homolog in *Euglena*, also has contacts at the dimer interface (Gahura, 2019).

The supposition that ATPaseTb9 is the main subunit required for dimerization is further strengthened by steady state western blot analyses of Tb9 RNAi induced cultures. In comparison to other subunits observed, knockdown of Tb9 leads to smaller differences in the abundance of $F_o$ and $F_1$ subunits. This reduced loss coincides with the BN Western blot data, suggesting there is a loss of dimers, but to a much lower extent a loss of monomers. A similar behavior was previously observed in mutants of yeast lacking the gene for either subunit g or subunit e, both of which were identified to be involved in dimerization and membrane curvature, but not significantly in monomer stability. When steady state western blots of these mutants were stained with $F_1$ β- or $F_1$ γ-antibodies, the signal intensity was comparable to wildtype (WT), indicating that monomer stability was not affected by presence of either subunit (Wagner et al., 2009). Conversely, Tb12 and Tb13 *T. brucei* RNAi cultures demonstrate an accumulation of $F_1$ subunits, while Tb1 and Tb2 ($F_o$) are being depleted, indicating a crucial involvement in monomer stability. Tb14 RNAi cultures show a similar behavior to Tb12 and Tb13, but abundancy of $F_1$ subunits remains rather stable, whereas Tb1 and Tb2 do not decrease as significantly. This suggests that Tb14 is less important for monomer stability and signifies further evidence of a potential involvement in dimerization, as observed by the preliminary structure elucidation (Gahura, 2019).

We performed an ATP production assay with samples from non-induced and induced cultures of the transfected Tb9 RNAi cell line in order to assess possible effects of dimerization on ATPase activity. Background ATP production was similar among all samples, whereas the ATP produced from OxPhos was decreased by 46% 2 days after induction and 27% 4 days after induction. The same experiment was performed for Tb12 RNAi cell cultures as a way to compare the effects of Tb9 depletion to a subunit which is known to affect monomer stability. Since lack of Tb12 disrupts both monomers and dimers, the decrease of ATP synthase activity should be more pronounced than for Tb9. Experimental data though suggests an increase in ATPase activity compared to the non-induced culture. This is however most likely due to a loading error, as the background ATP is also significantly reduced in the non-induced sample. Assuming the monomers are not disrupted by lack of Tb9, the experimental data would suggest that dimerization has a significant positive effect on the kinetics of the enzyme, which is in agreement with previous observations of ATPase monomer activity of *Podospora anserina* (Rampello et al., 2018). However, since ATP production assays produce variable bioluminescence intensities levels from experiment to experiment, a single experiment does not provide sufficient evidence. In order to strengthen this claim, the experiment would have

to be repeated. Also for better comparison of individual subunits, activity assays of WT cell cultures could be used for normalization.

All subunits under observation revealed a growth phenotype when RNAi was induced after at 3-4 days. The increased doubling times were similar for Tb12, Tb13 and Tb14 RNAi cultures, which is in agreement with their similar knockdown efficiencies determined by qPCR. The reduced growth rate was less pronounced for Tb9 RNAi cultures, although this might be due to a less significant depletion of the target transcript since this cell line has yet to be analyzed by qPCR. This growth phenotype is quite mild, which may suggest that a lack of ATP synthase dimers does not affect the rate of growth under these media conditions. However, we utilized sterile glucose-rich media containing SDM-79 to perform growth curves, which does not ideally represent conditions found in the procyclic host (tsetse fly). Expectedly, the growth phenotypes would be more pronounced in a low glucose environment, such as SDM-80, where the cells are more reliant on ATP synthase, as less ATP can be produced by SubPhos during glycolysis (Zíková et al., 2009).

In order to further explore the role of dimerization in ATP production and mt membrane ultrastructure, the shape of mt cristae in induced PF Tb9 RNAi cells can be observed by transmission electron microscopy. Without self-assembly of dimers into rows (Blum et al., 2019) the structure might significantly differ from wildtype *T. brucei* cells and might even resemble the cristae observed in BF cells. From these results, the precise contribution of ATP synthase dimers to cristae formation in *T. brucei* may be deduced.

# 5 Conclusion

In this study, we have analyzed the structural effects of depleting specific *T. brucei* $F_o$ ATP synthase subunits. The results demonstrate that a lack of the ATP synthase subunit Tb9 causes dimer instability, whereas the effect on monomer stability is much less pronounced. This Tb9 RNAi cell is therefore a powerful new tool that can be exploited to determine the significance of dimer formation in *T. brucei*. As a consequence, it might be revealed how ATPase dimers affect mt cristae ultrastructure and if there is an energetic benefit from the dimerization of the enzyme during oxidative phosphorylation.

# 6 References

Alsford, S., & Horn, D. (2008). Single-locus targeting constructs for reliable regulated RNAi and transgene expression in *Trypanosoma brucei*. *Molecular and Biochemical Parasitology*, *161*(1), 76–79.

Anselmi, C., Davies, K. M., & Faraldo-Gómez, J. D. (2018). Mitochondrial ATP synthase dimers spontaneously associate due to a long-range membrane-induced force. *The Journal of General Physiology*, *150*(5), 763–770.

Bacterial transformation. (2014). Retrieved from https://www.sigmaaldrich.com/technical-documents/protocols/biology/transformation.html

Baylis Scanlon, J. A., Al-Shawi, M. K., Le, N. P., & Nakamoto, R. K. (2007). Determination of the Partial Reactions of Rotational Catalysis in F1-ATPase†. *Biochemistry*, *46*(30), 8785–8797.

Blum, T. B., Hahn, A., Meier, T., Davies, K. M., & Kühlbrandt, W. (2019). Dimers of mitochondrial ATP synthase induce membrane curvature and self-assemble into rows. *Proceedings of the National Academy of Sciences*, *116*(10), 4250–4255.

Brun, R., Blum, J., Chappuis, F., & Burri, C. (2010). Human African trypanosomiasis. 375, 13.

Davies, K. M., Strauss, M., Daum, B., Kief, J. H., Osiewacz, H. D., Rycovska, A., Zickermann, V., & Kuhlbrandt, W. (2011). Macromolecular organization of ATP synthase and complex I in whole mitochondria. *Proceedings of the National Academy of Sciences*, *108*(34), 14121–14126.

Fenn, K., & Matthews, K. R. (2007). The cell biology of *Trypanosoma brucei* differentiation. *Current Opinion in Microbiology*, *10*(6), 539–546.

Gahura, O., Šubrtová, K., Váchová, H., Panicucci, B., Fearnley, I. M., Harbour, M. E., … Zíková, A. (2017). The F1-ATPase from *Trypanosoma brucei* is elaborated by three copies of an additional p18-subunit. *The FEBS Journal*, *285*(3), 614–628.

Gahura, O., (2019). [Structure of ATP synthase of *T. brucei*]. Unpublished raw data.

Garrido, C., Galluzzi, L., Brunet, M., Puig, P. E., Didelot, C., & Kroemer, G. (2006). Mechanisms of cytochrome c release from mitochondria. *Cell Death & Differentiation*, *13*(9), 1423–1433.

Glycogen, RNA grade. (n.d.). Retrieved from https://www.thermofisher.com/order/catalog/product/R0551

Gray, M. W. (2012). Mitochondrial Evolution. *Cold Spring Harbor Perspectives in Biology*, *4*(9), a011403.

Guo, H., Bueler, S. A., & Rubinstein, J. L. (2017). Atomic model for the dimeric $F_O$ region of mitochondrial ATP synthase. *Science*, *358*(6365), 936–940.

Guo, H., Suzuki, T., & Rubinstein, J. L. (2019). Structure of a bacterial ATP synthase. *ELife*, *8*.

Hannon, G. (2002). RNA interference. *Nature*, *418*, 244–251.

Hatefi, Y. (1985). The Mitochondrial Electron Transport and Oxidative Phosphorylation System. *Annual Review of Biochemistry*, *54*(1), 1015–1069.

He, J., Ford, H. C., Carroll, J., Douglas, C., Gonzales, E., Ding, S., Fearnley, I. M., & Walker, J. E. (2018). Assembly of the membrane domain of ATP synthase in human mitochondria. *Proceedings of the National Academy of Sciences*, *115*(12), 2988–2993.

Kaurov, I., Vancová, M., Schimanski, B., Cadena, L. R., Heller, J., Bílý, T., … Hashimi, H. (2018). The Diverged Trypanosome MICOS Complex as a Hub for Mitochondrial Cristae Shaping and Protein Import. *Current Biology*, *28*(21), 3393-3407.e5.

Klusch, N., Murphy, B. J., Mills, D. J., Yildiz, Ö., & Kühlbrandt, W. (2017). Structural basis of proton translocation and force generation in mitochondrial ATP synthase. *ELife*, *6*.

Kühlbrandt, W. (2019). Structure and Mechanisms of F-Type ATP Synthases. *Annual Review of Biochemistry*, *88*(1), 515–549.

Lenaz, G., & Genova, M. L. (2009). Mobility and function of Coenzyme Q (ubiquinone) in the mitochondrial respiratory chain. *Biochimica et Biophysica Acta (BBA) - Bioenergetics*, *1787*(6), 563–573.

Matthews, K. R. (2005). The developmental cell biology of *Trypanosoma brucei*. *Journal of Cell Science*, *118*(2), 283–290.

Minauro-Sanmiguel, F., Wilkens, S., & Garcia, J. J. (2005). Structure of dimeric mitochondrial ATP synthase: Novel F0 bridging features and the structural basis of mitochondrial cristae biogenesis. *Proceedings of the National Academy of Sciences*, *102*(35), 12356–12358.

Montgomery, M. G., Gahura, O., Leslie, A. G. W., Zíková, A., & Walker, J. E. (2018). ATP synthase from *Trypanosoma brucei* has an elaborated canonical F1-domain and conventional catalytic sites. *Proceedings of the National Academy of Sciences*, *115*(9), 2102–2107.

Mühleip, A. W., Dewar, C. E., Schnaufer, A., Kühlbrandt, W., & Davies, K. M. (2017). In situ structure of trypanosomal ATP synthase dimer reveals a unique arrangement of catalytic subunits. *Proceedings of the National Academy of Sciences*, *114*(5), 992–997.

Mühleip, A., McComas, S. E., & Amunts, A. (2019). Structure of a mitochondrial ATP synthase with bound native cardiolipin. *ELife*, *8*.

Nakamoto, R. K., Baylis Scanlon, J. A., & Al-Shawi, M. K. (2008). The rotary mechanism of the ATP synthase. *Archives of Biochemistry and Biophysics*, *476*(1), 43–50.

Neupane, P., Bhuju, S., Thapa, N., & Bhattarai, H. K. (2019). ATP Synthase: Structure, Function and Inhibition. *Biomolecular Concepts*, *10*(1), 1–10.

O'Connor, C., Adams, J. U., Fairman J. E. (2014). *Cell Biology for Seminars*. Retrieved from https://www.nature.com/scitable/ebooks/cell-biology-for-seminars-14760004/

Poon, S. K., Peacock, L., Gibson, W., Gull, K., & Kelly, S. (2012). A modular and optimized single marker system for generating *Trypanosoma brucei* cell lines expressing T7 RNA polymerase and the tetracycline repressor. *Open Biology*, *2*(2), 110037.

Pu, J., & Karplus, M. (2008). How subunit coupling produces the γ-subunit rotary motion in F1-ATPase. *Proceedings of the National Academy of Sciences*, *105*(4), 1192–1197.

Quintana-Cabrera, R., Mehrotra, A., Rigoni, G., & Soriano, M. E. (2018). Who and how in the regulation of mitochondrial cristae shape and function. *Biochemical and Biophysical Research Communications*, *500*(1), 94–101.

Rabl, R., Soubannier, V., Scholz, R., Vogel, F., Mendl, N., Vasiljev-Neumeyer, A., Körner, C., Jagasia, R., Keil, T., Baumeister, W., Cyrklaff, M., Neupert, W., & Reichert, A. S. (2009). Formation of cristae and crista junctions in mitochondria depends on antagonism between Fcj1 and Su *e* / *g*. *The Journal of Cell Biology*, *185*(6), 1047–1063.

Rampello, N. G., Stenger, M., Westermann, B., & Osiewacz, H. D. (2018). Impact of F1Fo-ATP-synthase dimer assembly factors on mitochondrial function and organismic aging. *Microbial Cell*, *5*(4), 198–207.

Smith, T. K., Bringaud, F., Nolan, D. P., & Figueiredo, L. M. (2017). Metabolic reprogramming during the *Trypanosoma brucei* life cycle. *F1000Research*, *6*, 683.

Srivastava, A. P., Luo, M., Zhou, W., Symersky, J., Bai, D., Chambers, M. G., … Mueller, D. M. (2018). High-resolution cryo-EM analysis of the yeast ATP synthase in a lipid membrane. *Science*, *360*(6389), eaas9699.

Šubrtová, K., Panicucci, B., & Zíková, A. (2015). ATPaseTb2, a Unique Membrane-bound FoF1-ATPase Component, Is Essential in Bloodstream and Dyskinetoplastic Trypanosomes. *PLOS Pathogens*, *11*(2), e1004660.

Wagner, K., Rehling, P., Sanjuán Szklarz, L. K., Taylor, R. D., Pfanner, N., & van der Laan, M. (2009). Mitochondrial F1Fo-ATP Synthase: The Small Subunits e and g Associate with Monomeric Complexes to Trigger Dimerization. *Journal of Molecular Biology*, *392*(4), 855–861.

Wittig, I., Braun, H. P. & Schägger, H. (2006). Blue native PAGE. Nature Protoc. 1, 418–428.

Yoshida, M., Muneyuki, E., & Hisabori, T. (2001). ATP synthase — a marvellous rotary engine of the cell. *Nature Reviews Molecular Cell Biology*, *2*(9), 669–677.

Zíková, A., Schnaufer, A., Dalley, A., Panigrahi, K., Stuart D. (2009). The FoF1-ATP synthase complex contains novel subunits and is essential for procyclic *Trypanosoma brucei*. *PLoS Pathogens*, 5(5).